PHYSICAL REVIEW D **92,** 095004 (2015)

Higgs data constraints on the minimal supersymmetric standard model

Kingman Cheung,[1,2,3] Jae Sik Lee,[3,4] and Po-Yan Tseng[1]

[1]*Department of Physics, National Tsing Hua University, Hsinchu 300, Taiwan*
[2]*Division of Quantum Phases and Devices, School of Physics, Konkuk University, Seoul 143-701, Republic of Korea*
[3]*Physics Division, National Center for Theoretical Sciences, Hsinchu 300, Taiwan*
[4]*Department of Physics, Chonnam National University, 300 Yongbong-dong, Buk-gu, Gwangju, 500-757, Republic of Korea*

(Received 31 July 2015; published 4 November 2015)

We perform global fits to the most recent data (after summer 2014) on Higgs boson signal strengths in the framework of the minimal supersymmetric standard model. We further impose the existing limits on the masses of charginos, staus, stops, and sbottoms together with the current Higgs mass constraint $|M_{H_1} - 125.5\ \mathrm{GeV}| < 6$ GeV. The heavy supersymmetric (SUSY) particles such as squarks enter into the loop factors of the Hgg and $H\gamma\gamma$ vertices, while other SUSY particles such as sleptons and charginos also enter into that of the $H\gamma\gamma$ vertex. We also take into account the possibility of other light particles, such as other Higgs bosons and neutralinos, into which the 125.5 GeV Higgs boson can decay. We use the data from the ATLAS, CMS, and the Tevatron, with existing limits on SUSY particles, to constrain on the relevant SUSY parameters. We obtain allowed regions in the SUSY parameter space of squark, slepton and chargino masses, and the μ parameter. We find that $|\Delta S^\gamma/S^\gamma_{\rm SM}| \lesssim 0.1$ at 68% confidence level when $M_{\tilde\chi_1^\pm} > 300$ GeV and $M_{\tilde\tau_1} > 300$ GeV, irrespective of the squarks masses. Furthermore, $|\Delta S^\gamma/S^\gamma_{\rm SM}| \lesssim 0.03$ when $M_{\tilde\chi_1^\pm,\tilde\tau_1} > 500$ GeV and $M_{\tilde t_1,\tilde b_1} \gtrsim 600$ GeV.

DOI: 10.1103/PhysRevD.92.095004 PACS numbers: 12.60.Jv, 14.80.Da

I. INTRODUCTION

The celebrated particle observed by the ATLAS [1] and the CMS [2] collaborations at the Large Hadron Collider (LHC) in July 2012 is more consistent with the standard model (SM) Higgs boson than any scalar particles appearing in other extensions of the SM [3,4], at least in terms of some statistical measures. The SM Higgs boson was proposed in 1960s [5] but only received the confirmation recently through its decays into $\gamma\gamma$ and $ZZ^* \to 4\ell$ modes.

Although the data on Higgs signal strengths are best described by the SM, the other extensions are still viable options to explain the data. Numerous activities occurred in the constraining of the SM boson [3,6–23], higher-dimension operators of the Higgs boson [24–29], the two-Higgs-doublet models [30–43], and in the supersymmetric framework [44–53]. A very recent update to all the data as of summer 2014 was performed in Ref. [4]. We shall describe the most significant change to the data set in Sec. III. In this work, we perform the fits in the framework of the minimal supersymmetric standard model (MSSM) to all the most updated data on Higgs signal strengths as of summer 2014.

In our previous analysis of the two-Higgs-doublet model (2HDM) [40], we do not specify which neutral Higgs boson is the observed Higgs boson, so that the whole scenario can be described by a small set of parameters. The bottom and leptonic Yukawa couplings are determined through the top Yukawa coupling, and the HWW coupling is determined via $\tan\beta$ and top Yukawa, so that a minimal set of parameters includes only $\tan\beta$ and the top Yukawa coupling. We can easily include the effects of the charged Higgs boson by the loop factor in the $H\gamma\gamma$ vertex and include possibly very light Higgs bosons by the factor $\Delta\Gamma_{\rm tot}$. Here we follow the same strategy for the global fits in the framework of the MSSM, the Higgs sector of which is the same as Type II of the 2HDM, in order to go along with a minimal set of parameters, unless we specifically investigate the spectrum of supersymmetric particles, e.g., the chargino mass.

In this work, we perform global fits in the MSSM under various initial conditions to the most updated data on Higgs boson signal strengths. A few specific features are summarized here.

(1) We use a minimal set of parameters without specifying the spectrum of the supersymmetry (SUSY) particles. For example, all up-, down-, and lepton-type Yukawa couplings and the gauge-Higgs coupling are given in terms of the top Yukawa coupling, $\tan\beta$, and κ_d, where κ_d is the radiative correction in the bottom Yukawa coupling defined later.
(2) Effects of heavy SUSY particles appear in the loop factors ΔS^g and ΔS^γ of the Hgg and $H\gamma\gamma$ vertices, respectively.
(3) Effects of additional light Higgs bosons or light neutralinos that the 125.5 GeV Higgs boson can decay into are included by the deviation $\Delta\Gamma_{\rm tot}$ in the Higgs boson width.

(4) CP-violating effects can occur in Yukawa couplings, which are quantified by the CP-odd part of the top-Yukawa coupling. Effects of other CP sources can appear in the loop factor of Hgg and $H\gamma\gamma$ vertices. We label them as ΔP^g and ΔP^γ, respectively. In Ref. [54], we have computed all the Higgs-mediated CP-violating contributions to the electric dipole moments (EDMs) and compared them to existing constraints from the EDM measurements of thallium, a neutron, mercury, and thorium monoxide. Nevertheless, we are content with CP-conserving fits in this work.

(5) We impose the existing limits of chargino and stau masses when we investigate specifically their effects on the vertex of $H\gamma\gamma$. The current limits on chargino and stau masses are [55]

$$M_{\tilde{\chi}^\pm} > 103.5\ \text{GeV}, \qquad M_{\tilde{\tau}_1} > 81.9\ \text{GeV}.$$

Similarly, the current limits for stop and sbottom masses quoted in Particle Data Group are [55]

$$M_{\tilde{t}_1} > 95.7\ \text{GeV}, \qquad M_{\tilde{b}_1} > 89\ \text{GeV},$$

which will be applied in calculating the effects in $H\gamma\gamma$ and Hgg vertices. Note that the current LHC limits on the stop and sbottom masses are $M_{\tilde{t}_1} > 650$ GeV and $M_{\tilde{b}_1} > 600$ GeV at 95% confidence level in a simplified model with $M_{\tilde{\chi}_1^0} = 0$ GeV [55]. However, there often exist underlying assumptions of search strategies and the mass of the lightest neutralino. Therefore, we conservatively take the above mass limits on the stops and sbottoms in most of the analysis.

(6) Since we shall try to find the implication of the current Higgs signal strength data on the SUSY spectrum, which in practice affects the lightest Higgs boson mass, we therefore also calculate the corresponding Higgs boson mass and impose the current Higgs mass constraint of $M_{H_1} \sim 125.5 \pm 6$ GeV, taking at a roughly 3-σ level.

The organization of the work is as follows. In the next section, we describe the convention and formulas for all the couplings used in this work. In Sec. III, we describe various CP-conserving fits and present the results. In Sec. IV, we specifically investigate the SUSY parameter space of charginos, staus, stops, and sbottoms. We put the synopsis and conclusions in Sec. V.

II. FORMALISM

For the Higgs couplings to SM particles, we assume that the observed Higgs boson is a generic CP-mixed state without carrying any definite CP-parity. We follow the conventions and notation of `CPsuperH` [56].

A. Yukawa couplings

The Higgs sector of the MSSM is essentially the same as Type II of the 2HDM. More details of the 2HDM can be found in Ref. [40]. In the MSSM, the first Higgs doublet couples to the down-type quarks and charged leptons, while the second Higgs doublet couples to the up-type quarks only. After both doublets take on vacuum-expectation values (VEV), we can rotate the neutral components ϕ_1^0, ϕ_2^0, and a into mass eigenstates $H_{1,2,3}$ through a mixing matrix O as follows:

$$(\phi_1^0, \phi_2^0, a)^T_\alpha = O_{\alpha i}(H_1, H_2, H_3)^T_i,$$

with the mass ordering $M_{H_1} \le M_{H_2} \le M_{H_3}$. We do not specify which Higgs boson is the observed one; in fact, it can be any of the $H_{1,2,3}$. We have shown in Ref. [40] that the bottom and lepton Yukawa couplings can be expressed in terms of the top Yukawa coupling in general 2HDM. We can therefore afford a minimal set of input parameters.

The effective Lagrangian governing the interactions of the neutral Higgs bosons with quarks and charged leptons is

$$\mathcal{L}_{H\bar{f}f} = -\sum_{f=u,d,l} \frac{g m_f}{2M_W} \sum_{i=1}^{3} H_i \bar{f}(g^S_{H_i\bar{f}f} + i g^P_{H_i\bar{f}f}\gamma_5) f. \qquad (1)$$

At the tree level, $(g^S, g^P) = (O_{\phi_1 i}/c_\beta, -O_{ai}\tan\beta)$ and $(g^S, g^P) = (O_{\phi_2 i}/s_\beta, -O_{ai}\cot\beta)$ for $f = (\ell, d)$ and $f = u$, respectively, and $\tan\beta \equiv v_2/v_1$ is the ratio of the VEVs of the two doublets. Threshold corrections to the down-type Yukawa couplings change the relation between the Yukawa coupling h_d and mass m_d as[1]

$$h_d = \frac{\sqrt{2} m_d}{v\cos\beta} \frac{1}{1+\kappa_d \tan\beta}. \qquad (2)$$

Thus, the Yukawa couplings of neutral Higgs-boson mass eigenstates H_i to the down-type quarks are modified as

$$\begin{aligned} g^S_{H_i\bar{d}d} &= \mathrm{Re}\left(\frac{1}{1+\kappa_d\tan\beta}\right)\frac{O_{\phi_1 i}}{\cos\beta} + \mathrm{Re}\left(\frac{\kappa_d}{1+\kappa_d\tan\beta}\right)\frac{O_{\phi_2 i}}{\cos\beta} \\ &\quad + \mathrm{Im}\left[\frac{\kappa_d(\tan^2\beta+1)}{1+\kappa_d\tan\beta}\right] O_{ai}, \\ g^P_{H_i\bar{d}d} &= -\mathrm{Re}\left(\frac{\tan\beta-\kappa_d}{1+\kappa_d\tan\beta}\right) O_{ai} + \mathrm{Im}\left(\frac{\kappa_d\tan\beta}{1+\kappa_d\tan\beta}\right)\frac{O_{\phi_1 i}}{\cos\beta} \\ &\quad - \mathrm{Im}\left(\frac{\kappa_d}{1+\kappa_d\tan\beta}\right)\frac{O_{\phi_2 i}}{\cos\beta}. \end{aligned} \qquad (3)$$

In the MSSM, neglecting the electroweak corrections and taking the most dominant contributions, κ_b can be split into [57]

[1] In general settings, κ_d and κ_s are usually the same, but κ_b could be very different because of the third-generation squarks. However, our main concern in this work is the third-generation Yukawa couplings. Thus, we shall focus on κ_b, although we are using the conventional notation κ_d.

$$\kappa_b = \epsilon_g + \epsilon_H,$$

where ϵ_g and ϵ_H are the contributions from the sbottom-gluino exchange diagram and from the stop-Higgsino diagram, respectively. Their explicit expressions are

$$\epsilon_g = \frac{2\alpha_s}{3\pi} M_3^* \mu^* I(m_{\tilde{b}_1}^2, m_{\tilde{b}_2}^2, |M_3|^2),$$
$$\epsilon_H = \frac{|h_t|^2}{16\pi^2} A_t^* \mu^* I(m_{\tilde{t}_1}^2, m_{\tilde{t}_2}^2, |\mu|^2),$$

where M_3 is the gluino mass, and h_t and A_t are the top-quark Yukawa and trilinear couplings, respectively.

B. Couplings to gauge bosons

Here we present the explicit forms of the Higgs couplings to the massive gauge bosons Z and $W^\pm$ and massless photons and gluons:

(i) Interactions of the Higgs bosons with the gauge bosons Z and $W^\pm$ are described by

$$\mathcal{L}_{HVV} = g M_W \left(W_\mu^+ W^{-\mu} + \frac{1}{2c_W^2} Z_\mu Z^\mu \right) \sum_i g_{H_i VV} H_i, \tag{4}$$

where

$$g_{H_i VV} = c_\beta O_{\phi_1 i} + s_\beta O_{\phi_2 i}. \tag{5}$$

(ii) Couplings to two photons: The amplitude for the decay process $H_i \to \gamma\gamma$ can be written as

$$\mathcal{M}_{\gamma\gamma H_i} = -\frac{\alpha M_{H_i}^2}{4\pi v} \left\{ S^\gamma(M_{H_i}) (\epsilon_{1\perp}^* \cdot \epsilon_{2\perp}^*) - P^\gamma(M_{H_i}) \frac{2}{M_{H_i}^2} \langle \epsilon_1^* \epsilon_2^* k_1 k_2 \rangle \right\}, \tag{6}$$

where $k_{1,2}$ are the momenta of the two photons and $\epsilon_{1,2}$ are the wave vectors of the corresponding photons, $\epsilon_{1\perp}^\mu = \epsilon_1^\mu - 2k_1^\mu (k_2 \cdot \epsilon_1)/M_{H_i}^2$, $\epsilon_{2\perp}^\mu = \epsilon_2^\mu - 2k_2^\mu (k_1 \cdot \epsilon_2)/M_{H_i}^2$, and $\langle \epsilon_1 \epsilon_2 k_1 k_2 \rangle \equiv \epsilon_{\mu\nu\rho\sigma} \epsilon_1^\mu \epsilon_2^\nu k_1^\rho k_2^\sigma$. The decay rate of $H_i \to \gamma\gamma$ is proportional to $|S^\gamma|^2 + |P^\gamma|^2$. The form factors are given by

$$S^\gamma(M_{H_i}) = 2 \sum_{f=b,t,\tau} N_C Q_f^2 g_{H_i \bar{f} f}^S F_{sf}(\tau_f) - g_{H_i VV} F_1(\tau_W) + \Delta S_i^\gamma,$$
$$P^\gamma(M_{H_i}) = 2 \sum_{f=b,t,\tau} N_C Q_f^2 g_{H_i \bar{f} f}^P F_{pf}(\tau_f) + \Delta P_i^\gamma, \tag{7}$$

where $\tau_x = M_{H_i}^2 / 4m_x^2$, and $N_C = 3$ for quarks and $N_C = 1$ for taus, respectively. In the MSSM, the factors ΔS_i^γ and ΔP_i^γ receive contributions from charginos, sfermions, and charged Higgs bosons,

$$\Delta S_i^\gamma = \sqrt{2} g \sum_{f=\tilde{\chi}_1^\pm, \tilde{\chi}_2^\pm} g_{H_i \bar{f} f}^S \frac{v}{m_f} F_{sf}(\tau_{if}) - \sum_{\tilde{f}_j = \tilde{t}_1, \tilde{t}_2, \tilde{b}_1, \tilde{b}_2, \tilde{\tau}_1, \tilde{\tau}_2} N_C Q_f^2 g_{H_i \tilde{f}_j^* \tilde{f}_j} \frac{v^2}{2m_{\tilde{f}_j}^2} F_0(\tau_{i\tilde{f}_j}) - g_{H_i H^+ H^-} \frac{v^2}{2M_{H^\pm}^2} F_0(\tau_{iH^\pm}),$$
$$\Delta P_i^\gamma = \sqrt{2} g \sum_{f=\tilde{\chi}_1^\pm, \tilde{\chi}_2^\pm} g_{H_i \bar{f} f}^P \frac{v}{m_f} F_{pf}(\tau_{if}), \tag{8}$$

where the couplings to charginos, sfermions, and charged Higgs are defined in the interactions

$$\mathcal{L}_{H\tilde{\chi}^+\tilde{\chi}^-} = -\frac{g}{\sqrt{2}} \sum_{i,j,k} H_k \overline{\tilde{\chi}_i^-} (g_{H_k \tilde{\chi}_i^+ \tilde{\chi}_j^-}^S + i\gamma_5 g_{H_k \tilde{\chi}_i^+ \tilde{\chi}_j^-}^P) \tilde{\chi}_j^-,$$
$$\mathcal{L}_{H\tilde{f}\tilde{f}} = v \sum_{f=u,d} g_{H_i \tilde{f}_j^* \tilde{f}_k} (H_i \tilde{f}_j^* \tilde{f}_k),$$
$$\mathcal{L}_{3H} = v \sum_{i=1}^{3} g_{H_i H^+ H^-} H_i H^+ H^-. \tag{9}$$

We shall describe the couplings of the Higgs boson to the charginos, sfermions, and charged Higgs boson a little later.

(iii) Couplings to two gluons: Similar to $H \to \gamma\gamma$, the amplitude for the decay process $H_i \to gg$ can be written as

$$\mathcal{M}_{ggH_i} = -\frac{\alpha_s M_{H_i}^2 \delta^{ab}}{4\pi v} \left\{ S^g(M_{H_i}) (\epsilon_{1\perp}^* \cdot \epsilon_{2\perp}^*) - P^g(M_{H_i}) \frac{2}{M_{H_i}^2} \langle \epsilon_1^* \epsilon_2^* k_1 k_2 \rangle \right\}, \tag{10}$$

where a and b (a, $b = 1$ to 8) are indices of the eight $SU(3)$ generators in the adjoint representation. The decay rate of $H_i \to gg$ is proportional to $|S^g|^2 + |P^g|^2$. The fermionic contributions and additional loop contributions from squarks in the MSSM to the scalar and pseudoscalar form factors are given by

$$S^g(M_{H_i}) = \sum_{f=b,t} g_{H_i \bar{f} f}^S F_{sf}(\tau_f) + \Delta S_i^g,$$
$$P^g(M_{H_i}) = \sum_{f=b,t} g_{H_i \bar{f} f}^P F_{pf}(\tau_f) + \Delta P_i^g, \tag{11}$$

with

$$\Delta S_i^g = -\sum_{\tilde{f}_j = \tilde{t}_1, \tilde{t}_2, \tilde{b}_1, \tilde{b}_2} g_{H_i \tilde{f}_j^* \tilde{f}_j} \frac{v^2}{4m_{\tilde{f}_j}^2} F_0(\tau_{i\tilde{f}_j}),$$
$$\Delta P_i^g = 0, \tag{12}$$

where the $\Delta P^g = 0$ because there are no colored SUSY fermions in the MSSM that can contribute to ΔP^g at one-loop level.

C. Interactions of neutral Higgs bosons with charginos, sfermions, and charged Higgs

The interactions between the Higgs bosons and charginos are described by the following Lagrangian:

$$\mathcal{L}_{H\tilde{\chi}^+\tilde{\chi}^-} = -\frac{g}{\sqrt{2}}\sum_{i,j,k} H_k \overline{\tilde{\chi}_i^-}(g^S_{H_k\tilde{\chi}_i^+\tilde{\chi}_j^-} + i\gamma_5 g^P_{H_k\tilde{\chi}_i^+\tilde{\chi}_j^-})\tilde{\chi}_j^-,$$

$$g^S_{H_k\tilde{\chi}_i^+\tilde{\chi}_j^-} = \frac{1}{2}\{[(C_R)_{i1}(C_L)^*_{j2}G_k^{\phi_1} + (C_R)_{i2}(C_L)^*_{j1}G_k^{\phi_2}] + [i\leftrightarrow j]^*\},$$

$$g^P_{H_k\tilde{\chi}_i^+\tilde{\chi}_j^-} = \frac{i}{2}\{[(C_R)_{i1}(C_L)^*_{j2}G_k^{\phi_1} + (C_R)_{i2}(C_L)^*_{j1}G_k^{\phi_2}] - [i\leftrightarrow j]^*\}, \tag{13}$$

where $G_k^{\phi_1} = (O_{\phi_1 k} - is_\beta O_{ak})$, $G_k^{\phi_2} = (O_{\phi_2 k} - ic_\beta O_{ak})$, i, $j = 1, 2$, and $k = 1$–3. The chargino mass matrix in the $(\tilde{W}^-, \tilde{H}^-)$ basis,

$$\mathcal{M}_C = \begin{pmatrix} M_2 & \sqrt{2}M_W c_\beta \\ \sqrt{2}M_W s_\beta & \mu \end{pmatrix}, \tag{14}$$

is diagonalized by two different unitary matrices $C_R\mathcal{M}_C C_L^\dagger = \mathrm{diag}\{M_{\tilde{\chi}_1^\pm}, M_{\tilde{\chi}_2^\pm}\}$, where $M_{\tilde{\chi}_1^\pm} \le M_{\tilde{\chi}_2^\pm}$. The chargino mixing matrices $(C_L)_{i\alpha}$ and $(C_R)_{i\alpha}$ relate the electroweak eigenstates to the mass eigenstates, via

$$\tilde{\chi}^-_{\alpha L} = (C_L)^*_{i\alpha}\tilde{\chi}^-_{iL}, \qquad \tilde{\chi}^-_{\alpha L} = (\tilde{W}^-, \tilde{H}^-)^T_L,$$
$$\tilde{\chi}^-_{\alpha R} = (C_R)^*_{i\alpha}\tilde{\chi}^-_{iR}, \qquad \tilde{\chi}^-_{\alpha R} = (\tilde{W}^-, \tilde{H}^-)^T_R. \tag{15}$$

The Higgs-sfermion-sfermion interaction can be written in terms of the sfermion mass eigenstates as

$$\mathcal{L}_{H\tilde{f}\tilde{f}} = v\sum_{f=u,d} g_{H_i\tilde{f}_j^*\tilde{f}_k}(H_i\tilde{f}_j^*\tilde{f}_k), \tag{16}$$

where

$$v g_{H_i\tilde{f}_j^*\tilde{f}_k} = (\Gamma^{\alpha\tilde{f}^*\tilde{f}})_{\beta\gamma} O_{\alpha i} U^{\tilde{f}^*}_{\beta j} U^{\tilde{f}}_{\gamma k},$$

with $\alpha = (\phi_1, \phi_2, a) = (1, 2, 3)$, β, $\gamma = L$, R, $i = (H_1, H_2, H_3) = (1, 2, 3)$, and j, $k = 1$, 2. The expressions for the couplings $\Gamma^{\alpha\tilde{f}^*\tilde{f}}$ are shown in Ref. [56]. The stop and sbottom mass matrices may conveniently be written in the $(\tilde{q}_L, \tilde{q}_R)$ basis as

$$\tilde{\mathcal{M}}_q^2 = \begin{pmatrix} M^2_{\tilde{Q}_3} + m_q^2 + c_{2\beta}M_Z^2(T_z^q - Q_q s_W^2) & h_q^* v_q(A_q^* - \mu R_q)/\sqrt{2} \\ h_q v_q(A_q - \mu^* R_q)/\sqrt{2} & M^2_{\tilde{R}_3} + m_q^2 + c_{2\beta}M_Z^2 Q_q s_W^2 \end{pmatrix}, \tag{17}$$

with $q = t, b$, $R = U, D$, $T_z^t = -T_z^b = 1/2$, $Q_t = 2/3$, $Q_b = -1/3$, $v_b = v_1$, $v_t = v_2$, $R_b = \tan\beta = v_2/v_1$, $R_t = \cot\beta$, and h_q is the Yukawa coupling of the quark q. On the other hand, the stau mass matrix is written in the $(\tilde{\tau}_L, \tilde{\tau}_R)$ basis as

$$\tilde{\mathcal{M}}_\tau^2 = \begin{pmatrix} M^2_{\tilde{L}_3} + m_\tau^2 + c_{2\beta}M_Z^2(s_W^2 - 1/2) & h_\tau^* v_1(A_\tau^* - \mu\tan\beta)/\sqrt{2} \\ h_\tau v_1(A_\tau - \mu^*\tan\beta)/\sqrt{2} & M^2_{\tilde{E}_3} + m_\tau^2 + c_{2\beta}M_Z^2 s_W^2 \end{pmatrix}. \tag{18}$$

The 2×2 sfermion mass matrix $\tilde{M}_f^2$ for $f = t$, b, and τ is diagonalized by a unitary matrix $U^{\tilde{f}}$: $U^{\tilde{f}\dagger}\tilde{M}_f^2 U^{\tilde{f}} = \mathrm{diag}(m^2_{\tilde{f}_1}, m^2_{\tilde{f}_2})$ with $m^2_{\tilde{f}_1} \le m^2_{\tilde{f}_2}$. The mixing matrix $U^{\tilde{f}}$ relates the electroweak eigenstates $\tilde{f}_{L,R}$ to the mass eigenstates $\tilde{f}_{1,2}$, via

$$(\tilde{f}_L, \tilde{f}_R)^T_\alpha = U^{\tilde{f}}_{\alpha i}(\tilde{f}_1, \tilde{f}_2)^T_i.$$

Interactions between the Higgs bosons and the charged Higgs boson can be found in Ref. [40].

III. DATA, FITS, AND RESULTS

A. Data

Our previous works [3,40,54] were performed with the data of Summer 2013. Very recently, we have also updated the model-independent fits using the data of Summer 2014 [4]. The whole set of Higgs strength data on $H\to\gamma\gamma$, $ZZ^*\to 4\ell$, $WW^*\to\ell\nu\ell\nu$, $\tau\tau$, and $b\bar{b}$ are listed in Ref. [4]. The most significant changes since Summer 2013 are the $H\to\gamma\gamma$ data from both ATLAS and CMS. The ATLAS Collaboration updated their best-measured value from $\mu_{ggH+ttH} = 1.6\pm 0.4$ to $\mu_{\rm inclusive} = 1.17\pm 0.27$ [58], while the CMS $H\to\gamma\gamma$ data entertained a very dramatic change from $\mu_{\rm untagged} = 0.78^{+0.28}_{-0.26}$ to $\mu_{ggH} = 1.12^{+0.37}_{-0.32}$ [59]. Other notable differences can be found in Ref. [4]. The $\chi^2_{\rm SM}/{\rm d}.o.f.$ for the SM is now at 16.76/29, which corresponds to a p value of 0.966.

B. *CP*-Conserving fits

We consider the *CP*-conserving (CPC) MSSM and use the most updated Higgs boson signal strengths to constrain a minimal set of parameters under various conditions. Regarding the ith Higgs boson H_i as the candidate for the 125 GeV Higgs boson, the varying parameters are:

(i) the up-type Yukawa coupling $C_u^S \equiv g^S_{H_i\bar{u}u} = O_{\phi_2 i}/s_\beta$ [see Eq. (1)],
(ii) the ratio of the VEVs of the two Higgs doublets $\tan\beta \equiv v_2/v_1$,
(iii) the parameter κ_d (assumed real) quantifying the modification between the down-type quark mass and Yukawa coupling due to radiative corrections, as shown in Eq. (2),
(iv) $\Delta S^\gamma \equiv \Delta S_i^\gamma$ as in Eq. (8)
(v) $\Delta S^g \equiv \Delta S_i^g$ as in Eq. (12), and
(vi) the deviation in the total decay width of the observed Higgs boson: $\Delta\Gamma_{\rm tot}$.

The down-type and lepton-type Yukawa and the gauge-Higgs couplings are derived as

$$C_d^S \equiv g^S_{H_i\bar{d}d} = \left(\frac{O_{\phi_1 i} + \kappa_d O_{\phi_2 i}}{1+\kappa_d \tan\beta}\right)\frac{1}{\cos\beta},$$
$$C_\ell^S \equiv g^S_{H_i\bar{\ell}\ell} = \frac{O_{\phi_1 i}}{\cos\beta},$$
$$C_v \equiv g_{H_iVV} = c_\beta O_{\phi_1 i} + s_\beta O_{\phi_2 i} \qquad (19)$$

with

$$O_{\phi_1 i} = \pm\sqrt{1 - s_\beta^2 (C_u^S)^2}, \qquad O_{\phi_2 i} = C_u^S s_\beta. \qquad (20)$$

In place of $\tan\beta$, we can use C_v as a varying parameter, and then $\tan\beta(t_\beta)$ would be determined by

$$t_\beta^2 = \frac{(1-C_v^2)}{(C_u^S - C_v)^2} = \frac{(1-C_v^2)}{[(C_u^S-1)+(1-C_v)]^2}. \qquad (21)$$

We note that $t_\beta = \infty$ when $(C_u^S - 1) = -(1-C_v) < 0$,[2] while $t_\beta = 1$ when $(C_u^S-1) = \pm\sqrt{1-C_v^2} - (1-C_v)$. Therefore, t_β changes from ∞ to 1 when (C_u^S-1) deviates from $-(1-C_v)$ by the amount of $\pm\sqrt{1-C_v^2}$. This implies that the value of t_β becomes more and more sensitive to the deviation of C_u^S from 1 as C_v approaches to its SM value 1.

We are going to perform the following three categories of CPC fits varying the stated parameters while keeping the others at their SM values.

(1) CPC.II
  (a) CPC.II.2: C_u^S, $\tan\beta$ ($\kappa_d = \Delta\Gamma_{\rm tot} = \Delta S^\gamma = \Delta S^g = 0$)
  (b) CPC.II.3: C_u^S, $\tan\beta$, κ_d ($\Delta\Gamma_{\rm tot} = \Delta S^\gamma = \Delta S^g = 0$)
  (c) CPC.II.4: C_u^S, $\tan\beta$, κ_d, $\Delta\Gamma_{\rm tot}$ ($\Delta S^\gamma = \Delta S^g = 0$)
(2) CPC.III
  (a) CPC.III.3: C_u^S, $\tan\beta$, ΔS^γ ($\kappa_d = \Delta\Gamma_{\rm tot} = \Delta S^g = 0$)
  (b) CPC.III.4: C_u^S, $\tan\beta$, ΔS^γ, κ_d ($\Delta\Gamma_{\rm tot} = \Delta S^g = 0$)
  (c) CPC.III.5: C_u^S, $\tan\beta$, ΔS^γ, κ_d, $\Delta\Gamma_{\rm tot}$ ($\Delta S^g = 0$)
(3) CPC.IV
  (a) CPC.IV.4: C_u^S, $\tan\beta$, ΔS^γ, ΔS^g ($\kappa_d = \Delta\Gamma_{\rm tot} = 0$)
  (b) CPC.IV.5: C_u^S, $\tan\beta$, ΔS^γ, ΔS^g, κ_d ($\Delta\Gamma_{\rm tot} = 0$)
  (c) CPC.IV.6: C_u^S, $\tan\beta$, ΔS^γ, ΔS^g, κ_d, $\Delta\Gamma_{\rm tot}$

The basic varying parameters of the CPC.II fits are C_u^S and $\tan\beta$; those of the CPC.III fits are C_u^S, $\tan\beta$, and ΔS^γ; and those of the CPC.IV fits C_u^S, $\tan\beta$, ΔS^γ, and ΔS^g. Each category of CPC fits includes three fits; the second fit adds κ_d to the set of varying parameters, and $\Delta\Gamma_{\rm tot}$ is further varied in the third one. The Arabic number at the end of each label denotes the total number of varying parameters.

The ΔS^γ is the deviation in the $H\gamma\gamma$ vertex factor other than the effects of changing the Yukawa and gauge-Higgs couplings, and it receives contributions from any exotic particles running in the triangular loop, for example, the charginos, charged Higgs bosons, sleptons, and squarks in the MSSM. Here we are content with a varying ΔS^γ without specifying the particle spectrum of the MSSM. Later in the next section, we shall specifically investigate the effects of charginos, staus, stops, and sbottoms.

In the MSSM, ΔS^g receives contributions only from colored SUSY particles or squarks running in the Hgg vertex. The current limits on squark masses are in general above TeV such that ΔS^g is expected to be small. Nevertheless, we do not restrict the size of ΔS^g in this fit in order to see the full effect of ΔS^g.

The parameter κ_d arises from the loop corrections to the down-type Yukawa couplings. It changes the relation between the mass and the Yukawa coupling of the down-type quarks. We limit the range of $|\kappa_d| < 0.1$ as it is much smaller than 0.1 in most of the MSSM parameter space.

Although the charginos are constrained to be heavier than 103.5 GeV and sleptons constrained to be heavier than 81.9 GeV [55], there are still possibilities that the decays of the 125.5 GeV Higgs boson into neutralinos and another neutral Higgs boson are kinematically allowed. These channels have not been explicitly searched for, but we can take them into account by the deviation $\Delta\Gamma_{\rm tot}$ in the total decay width of the observed Higgs boson.

The best-fit points for the fits are summarized in Table I. We see that the p values of the CPC.II.2, CPC.III.3, and CPC.IV.4 fits are the highest in each category. Also, the p value of the CPC.III.3 fit is slightly higher than that of the CPC.IV.4 fit, followed by the CPC.II.2 fit.

C. Results

Before we present descriptions of the confidence regions and the correlations among the fitting parameters C_u^S, $\tan\beta$, ΔS^γ, ΔS^g, κ_d, and $\Delta\Gamma_{\rm tot}$, we look into the behavior of $\Delta\chi^2$ vs C_u^S in each category of fits. In the CPC.II fits, the minimum χ^2 values are 16.74 (CPC.II.2, CPC.II.3) and 16.72 (CPC.II.4) (see Table I), and $\Delta\chi^2$ vs C_u^S are shown in the upper row of Fig. 1. The minima are located at

[2]Note $C_v \leq 1$ and is positive definite in our convention.

TABLE I. The best-fit values for various CPC fits. The SM chi-square per degree of freedom is $\chi^2_{\rm SM}/{\rm d.o.f.} = 16.76/29$, and the p value $= 0.966$.

				Best-fit values								
Fits	χ^2	χ^2/dof	p-value	C_u^S	$\tan\beta$	ΔS^γ	ΔS^g	κ_d	$\Delta\Gamma_{\rm tot}$	C_v	C_d^S	C_ℓ^S
CPC.II.2	16.74	0.620	0.937	1.011	0.111	⋯	⋯	⋯	⋯	1.000	1.000	1.000
CPC.II.3	16.74	0.644	0.917	1.011	0.194	⋯	⋯	0.099	⋯	1.000	1.000	1.000
CPC.II.4	16.72	0.669	0.892	1.023	0.312	⋯	⋯	−0.079	0.103	1.000	0.997	0.998
CPC.III.3	15.50	0.596	0.947	−0.930	0.194	2.326	⋯	⋯	⋯	0.932	1.003	1.003
CPC.III.4	15.48	0.619	0.929	−0.948	0.180	2.402	⋯	−0.097	⋯	0.940	1.036	1.002
CPC.III.5	15.43	0.643	0.907	1.061	0.100	−0.938	⋯	0.100	0.557	1.000	1.000	1.000
CPC.IV.4	14.85	0.594	0.945	−1.219	0.154	2.893	1.547	⋯	⋯	0.943	0.994	0.994
	14.85	0.594	0.945	−1.219	0.154	2.893	0.204	⋯	⋯	0.943	0.994	0.994
CPC.IV.5	14.83	0.618	0.926	−1.224	0.164	2.902	1.540	0.088	⋯	0.935	0.962	0.993
	14.83	0.618	0.926	−1.225	0.164	2.902	0.217	0.088	⋯	0.935	0.962	0.993
CPC.IV.6	14.83	0.645	0.901	−1.213	0.173	2.868	1.528	0.082	−0.071	0.929	0.962	0.993
	14.83	0.645	0.901	−1.213	0.173	2.870	0.213	0.079	−0.075	0.929	0.963	0.993
	14.83	0.645	0.901	1.022	2.600	−1.228	−0.180	0.005	−0.839	0.782	−0.811	−0.837
	14.83	0.645	0.901	1.022	2.600	−1.228	−1.288	0.005	−0.840	0.782	−0.811	−0.837

$C_u^S = 1.011$ (CPC.II.2, CPC.II.3) and $C_u^S = 1.023$ (CPC.II.4), and the second local minima are developed around $C_u^S = -1$ but with $\Delta\chi^2 \gtrsim 5$. It is clear that $C_u^S \approx 1$ is preferred much more than the negative values. The $\Delta\chi^2$ dependence on C_u^S hardly changes by varying κ_d as shown in the upper-middle frame. With $\Delta\Gamma_{\rm tot}$ varying further, we observe the dependence of $\Delta\chi^2$ on C_u^S becomes broader by extending to the regions of $|C_u^S| > 1$ as shown in the upper-right frame. We also observe that the second local minimum around $C_u^S = -1$ disappears when $\tan\beta \gtrsim 0.6$.

In the CPC.III fits, the minimum χ^2 values are 15.50 (CPC.III.3), 15.48 (CPC.III.4), and 15.43 (CPC.III.5), see Table I, and $\Delta\chi^2$ vs C_u^S are shown in the middle row of Fig. 1. The minima are located at $C_u^S = -0.930$ (CPC.III.3), $C_u^S = -0.948$ (CPC.III.4), and $C_u^S = 1.061$ (CPC.III.5), and the second local minima are developed around $C_u^S = 1$ (CPC.III.3 and CPC.III.4) and $C_u^S = -1$ (CPC.III.5), respectively. In contrast to the CPC.II fits, the $\Delta\chi^2$ difference between the true and local minima is tiny, $\Delta\chi^2|_{\rm local} - \Delta\chi^2|_{\rm true} \lesssim 0.2$; see Table II. The $\Delta\chi^2$ dependence on C_u^S hardly changes by varying κ_d additionally (shown in the middle-middle frame), but when $\Delta\Gamma_{\rm tot}$ is varied further, the dependence of $\Delta\chi^2$ on C_u^S becomes broader, the same as the CPC.II fits (see the middle-right frame). We observe the true/local minima around $C_u^S = -1$ disappear when $\tan\beta \gtrsim 0.6$.

In the CPC.IV fits, the minimum χ^2 values are 14.85 (CPC.IV.4), 14.83 (CPC.IV.5 and CPC.IV.6), see Table I, and $\Delta\chi^2$ vs C_u^S are shown in the lower row of Fig. 1. The minima are located at $C_u^S = -1.219$ (CPC.IV.4), $C_u^S = -1.225$ (CPC.IV.5), and $C_u^S = -1.213$, 1.022 (CPC.IV.6). The second local minima are developed for CPC.IV.4 and CPC.IV.5 at $C_u^S = 1$; see Table II. Similar to the CPC.III fits, the $\Delta\chi^2$ difference between the true and local minima is tiny for CPC.IV.4 and CPC.IV.5, $\Delta\chi^2|_{\rm local} - \Delta\chi^2|_{\rm true} \sim 0.4$; see Table II. On the other hand, in contrast to the CPC.III fits, any values of C_u^S between −2 and 2 are allowed at 2-σ level and higher. The behavior of $\Delta\chi^2$ by additionally varying κ_d and $\Delta\Gamma_{\rm tot}$ is the same as in the previous cases. We again observe the true minima around $C_u^S = -1$ disappear when $\tan\beta \gtrsim 0.6$.

We show the confidence-level regions on the $(C_u^S, \tan\beta)$ plane for three categories of CPC fits: CPC.II (upper row), CPC.III (middle row), and CPC.IV (lower row) in Fig. 2. The confidence level (C.L.) regions shown are for $\Delta\chi^2 \le 2.3$ (red), 5.99 (green), and 11.83 (blue) above the minimum, which correspond to C.L.s of 68.3%, 95%, and 99.7%, respectively. The best-fit point is denoted by the triangle. We observe that the plots are very close to those of Type II of the 2HDM [40], though the regions in general shrink by small amounts. First of all, the vertical 68.3% confidence (red) regions around $C_u^S = 1$ can be understood from Eq. (21) by observing that the value of t_β changes from ∞ to 1 when $(C_u^S - 1)$ deviates from $-(1 - C_v)$ by the amount of $\pm\sqrt{1 - C_v^2}$ and there are generally many points around $C_v = 1$ as shown in Fig. 3.

In each category of fits, Fig. 1 is helpful to understand the basic behavior of the C.L. regions as C_u^S is varied. In the CPC.II fits, the region around $C_u^S = 1$ is much more preferred. The negative C_u^S values are not allowed at 68% C.L. In the CPC.III fits, the region around $C_u^S = -1$ falls into the stronger 68.3% C.L., but $C_u^S = 0$ is not allowed even at 99.7% C.L. On the other hand, the whole range of $-2 < C_u^S < 2$ is allowed at 95% C.L. for the CPC.IV fits though not at 68.3% C.L. In all the fits, the negative values of C_u^S are not allowed at 95% C.L. when $\tan\beta \gtrsim 0.5$ is imposed, which is in general required by the perturbativity of the top-quark Yukawa coupling. The C.L. regions hardly change by varying κ_d additionally, but the

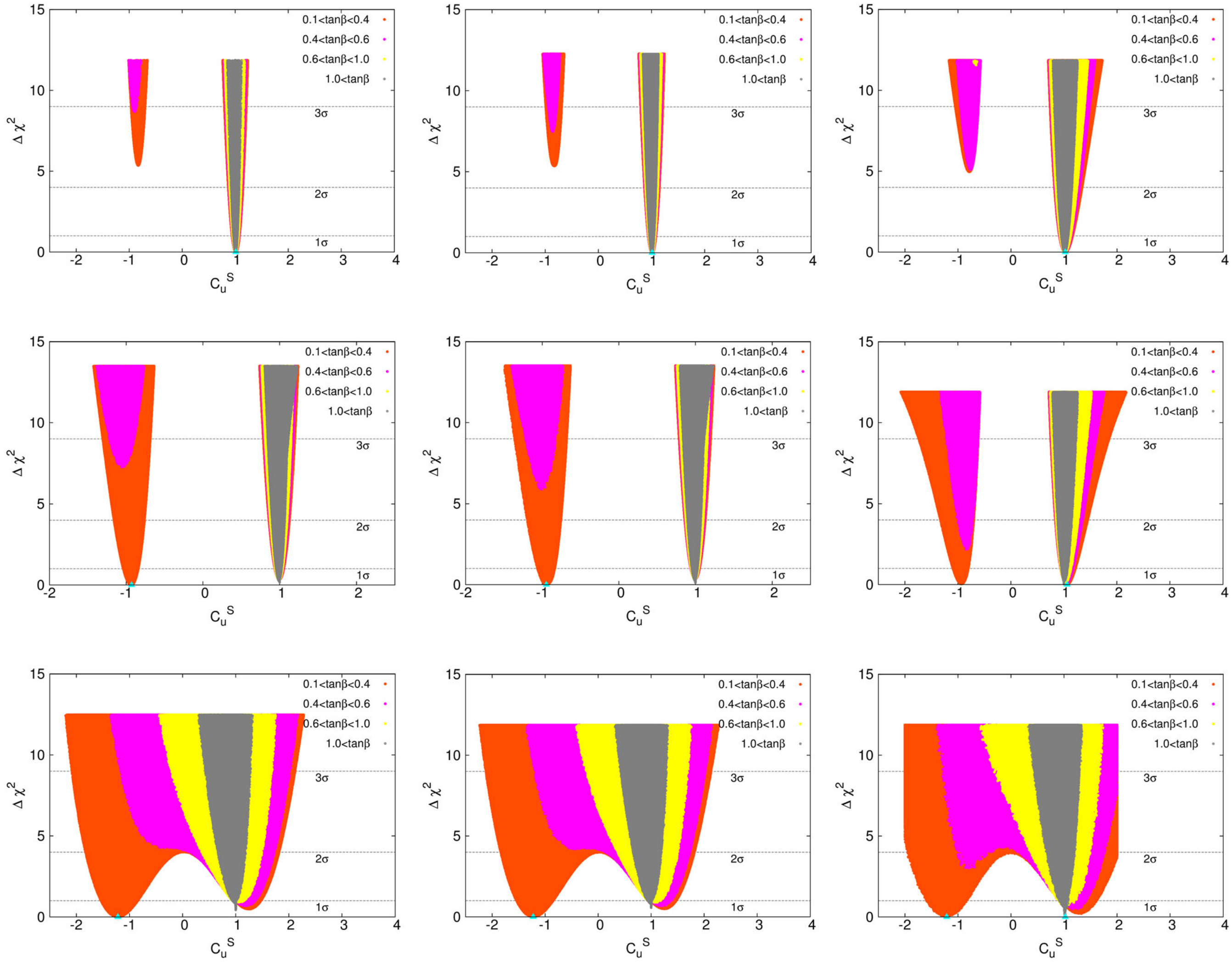

FIG. 1 (color online). Plots of $\Delta\chi^2$ vs C_u^S for three categories of CPC fits: CPC.II (upper row), CPC.III (middle row), and CPC.IV (lower row). The left frames show the cases of CPC.II.2 (varying C_u^S, $\tan\beta$), CPC.III.3 (varying C_u^S, $\tan\beta$, ΔS^γ), and CPC.IV.4 (varying C_u^S, $\tan\beta$, ΔS^γ, ΔS^g). In the middle frames, the cases CPC.II.3, CPC.III.4, and CPC.IV.5 are shown by adding κ_d to the corresponding set of varying parameters. The right frames are for the cases of CPC.II.4, CPC.III.5, and CPC.IV.6 in which $\Delta\Gamma_{\rm tot}$ is further varied. In each frame, each different color corresponds to a different range of $\tan\beta$: $0.1 < \tan\beta < 0.4$ (red), $0.4 < \tan\beta < 0.6$ (magenta), $0.6 < \tan\beta < 1$ (yellow), and $1 < \tan\beta$ (gray).

C.L. regions can extend to the regions of $|C_u^S| > 1$ by further varying $\Delta\Gamma_{\rm tot}$.

The C.L. regions on the (C_u^S, C_v) plane are shown in Fig. 3 for the three categories of CPC fits: CPC.II (upper row), CPC.III (middle row), and CPC.IV (lower row). The C.L. regions are labeled in the same way as in Fig. 2. We observe $C_v \gtrsim 0.75$ at 68.3% C.L. except in the CPC.IV.6 fit. Otherwise, one may make similar

TABLE II. The other local minima for various CPC fits.

Fits	χ^2	χ^2/dof	p-value	Best-fit values								
				C_u^S	$\tan\beta$	ΔS^γ	ΔS^g	κ_d	$\Delta\Gamma_{\rm tot}$	C_v	C_d^S	C_ℓ^S
CPC.III.3	15.68	0.603	0.944	1.000	34.58	−0.853	⋯	⋯	⋯	1.000	1.039	1.039
CPC.III.4	15.59	0.624	0.926	0.999	9.332	−1.026	⋯	−0.006	⋯	0.976	−1.170	−1.051
CPC.IV.4	15.23	0.609	0.936	1.000	5.681	−1.127	−0.057	⋯	⋯	0.940	−1.002	−1.002
	15.23	0.609	0.936	1.000	5.695	−1.126	−1.395	⋯	⋯	0.940	−1.002	−1.002
CPC.IV.5	15.22	0.634	0.914	1.000	5.423	−1.128	−0.062	0.002	⋯	0.934	−0.980	−0.999
	15.22	0.634	0.914	1.000	5.429	−1.127	−1.387	0.002	⋯	0.934	−0.980	0.999

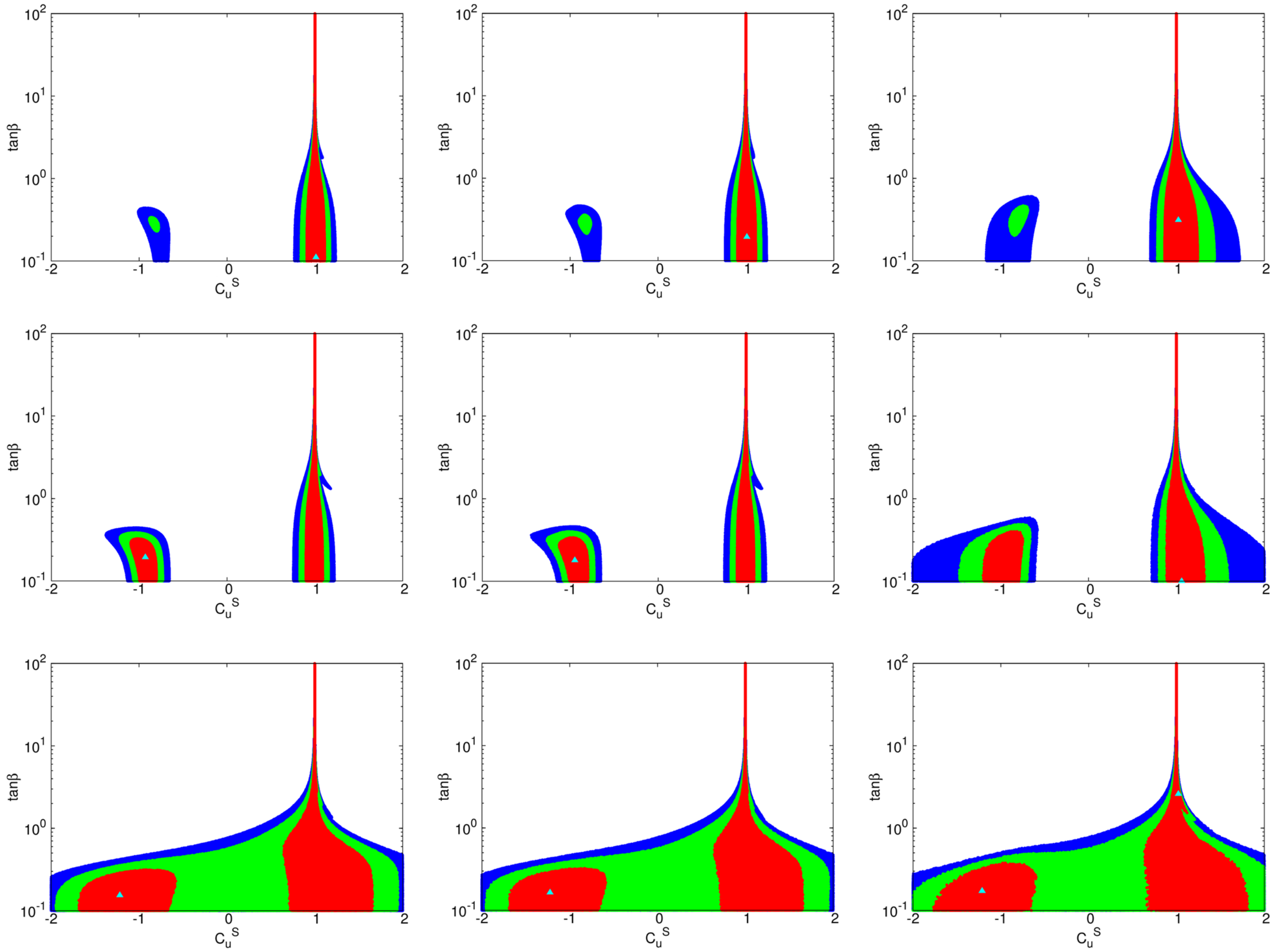

FIG. 2 (color online). The confidence-level regions on the (C_u^S, $\tan\beta$) plane for three categories of CPC fits: CPC.II (upper row), CPC.III (middle row), and CPC.IV (lower row) fits. The left frames show the cases of CPC.II.2 (varying C_u^S, $\tan\beta$), CPC.III.3 (varying C_u^S, $\tan\beta$, ΔS^γ), and CPC.IV.4 (varying C_u^S, $\tan\beta$, ΔS^γ, ΔS^g). In the middle frames, the cases CPC.II.3, CPC.III.4, and CPC.IV.5 are shown by adding κ_d to the corresponding set of varying parameters. The right frames are for the cases of CPC.II.4, CPC.III.5, and CPC.IV.6 in which $\Delta\Gamma_{\rm tot}$ is further varied. The confidence regions shown are for $\Delta\chi^2 \leq 2.3$ (red), 5.99 (green), and 11.83 (blue) above the minimum, which correspond to confidence levels of 68.3%, 95%, and 99.7%, respectively. The best-fit point is denoted by the triangle.

observations as in Fig. 2 for the behavior of the C.L. regions as C_u^S is varied.

Figure 4 shows the C.L. regions on the (C_u^S, C_d^S) plane in the same format as Fig. 2. $C_d^S \approx 1$ is preferred except for the CPC.IV.6 fit, in which the best-fit values of C_d^S are about 0.96 and -0.81 when $C_u^S \sim -1.2$ and 1.0, respectively; see Table I. Nevertheless, the difference in $\Delta\chi^2$ between the true minima and the local minimum around the SM limit $(C_u^S, C_d^S) = (1, 1)$ is small. The C.L. regions, centered around the best-fit values, significantly expand as the fit progresses from CPC.II to CPC.III and from CPC.III to CPC.IV, as well as by adding $\Delta\Gamma_{\rm tot}$ to the set of varying parameters.

We show the C.L. regions on the (C_d^S, C_ℓ^S) plane in Fig. 5. The format is the same as in Fig. 2. At tree level without including κ_d, $C_\ell^S = C_d^S = O_{\phi_1 i}/\cos\beta$ as clearly seen in the left frames, and the true and local minima are located at $(C_d^S, C_\ell^S) = (1, 1)$ and $(-1, -1)$. The tree-level relation is modified by introducing κ_d, and the local minima around $(C_d^S, C_\ell^S) = (-1, 1)$ are developed as shown in the middle frames. Further varying $\Delta\Gamma_{\rm tot}$, we observe that $C_d^S = 0$ is allowed at the 99.7% C.L. but $|C_\ell^S| > 0$ always; see the right frames.

The C.L. regions involved with κ_d are shown in the left and middle frames of Fig. 6 for the CPC.II (upper), CPC.III (middle), and CPC.IV (lower) fits. We see any value of κ_d between -0.1 and 0.1 is allowed.

Note that in the most recent update [4] when $\Delta\Gamma_{\rm tot}$ is the only parameter allowed to vary, the fitted value of $\Delta\Gamma_{\rm tot}$ is consistent with zero and is constrained by

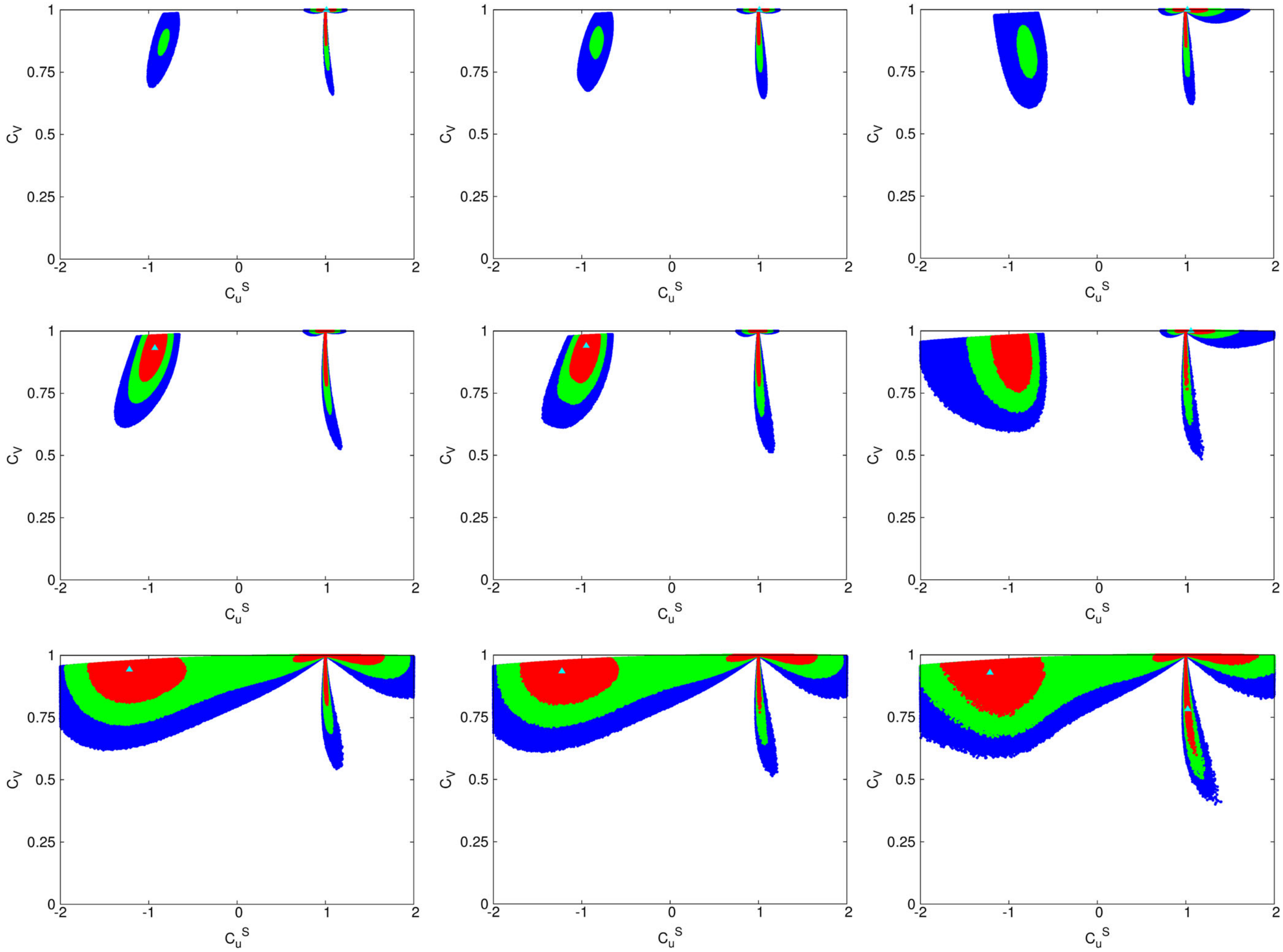

FIG. 3 (color online). The same as in Fig. 2 but on the (C_u^S, C_v) plane.

$\Delta\Gamma_{\rm tot} < 0.97$ MeV at 95% C.L. From the right frames of Fig. 6, we observe that the range of $\Delta\Gamma_{\rm tot}$ at 95% C.L. (green region) varies from -2.4 MeV to 3.3 MeV (CPC.II.4) and -2.9 MeV to 5.6 MeV (CPC.III.5 and CPC.IV.6). Such a large range is not very useful in constraining the exotic decay branching ratio of the Higgs boson. Usually we have to limit the number of varying parameters to be small enough to draw a useful constraint on $\Delta\Gamma_{\rm tot}$.

We show the C.L. regions on the (C_u^S, ΔS^γ) plane in Fig. 7 for the CPC.III (upper) and CPC.IV (lower) fits. In the CPC.III fits, the range of ΔS^γ is from $-2.5(1)$ to $0.3(3.7)$ at 68.3% C.L. for the positive (negative) C_u^S. In the CPC.IV fits, the range is a bit widened.

In Fig. 8, we show the C.L. regions of the CPC.IV fits on the (C_u^S, ΔS^g) (upper) and (ΔS^γ, ΔS^g) (lower) planes. We found that there are two bands of ΔS^g allowed by data, which are consistent with the results in the model-independent fits [3]. In the plots of ΔS^γ vs ΔS^g, there are four almost degenerate solutions to the local minimum of χ^2, which only differ from one another by a very small amount. It happens because ΔS^γ and ΔS^g satisfy a set of elliptical-type equations, which imply two solutions for each of ΔS^γ and ΔS^g [3].

A quick summary of the CPC fits is in order here. The confidence regions in various fits are similar to Type II of the 2HDM. When κ_d and $\Delta\Gamma_{\rm tot}$ (not investigated in the previous 2HDM fits) are allowed to vary, the confidence regions are slightly and progressively enlarged due to more varying parameters. Especially the linear relation between C_d^S and C_ℓ^S are "diffused" when κ_d varies between ± 0.1 as shown in Eq. (19). The two possible solutions for ΔS^γ in the CPC.III and CPC.IV cases are consistent with what we have found in previous works [3,40]. The best-fit point of each fit is shown in Table I with the corresponding p value. It is clear that the SM fit provides the best p value in consistence with our previous works [3,4,40]. Among the fits other than the SM one, the CPC.III.3 fit gives the smallest χ^2 per degree of freedom and thus the largest p value. It demonstrates that the set of parameters consisting of the top-Yukawa coupling C_u^S, $\tan\beta$ or equivalently the gauge-Higgs coupling C_v, and ΔS^γ is the minimal set of parameters that gives the best description

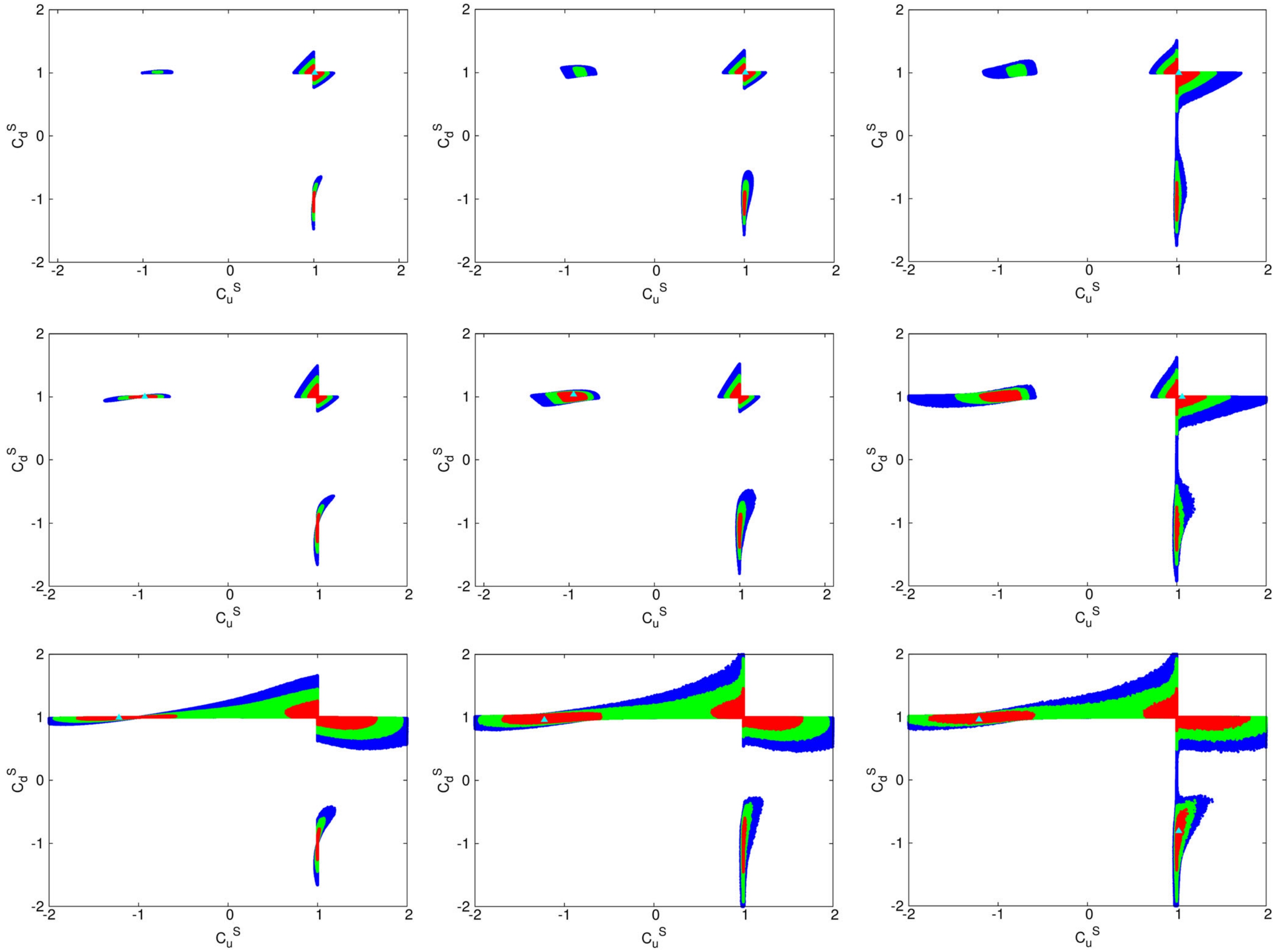

FIG. 4 (color online). The same as in Fig. 2 but on the (C_u^S, C_d^S) plane.

of the data, other than the SM. In this fit, the best-fit value of C_v is 0.93, which is very close to the SM value, while C_u^S takes on a negative value −0.93. The effects of the negative C_u^S coupling are compensated by those of a relatively large $\Delta S^\gamma = 2.3$. The derived C_d^S and C_ℓ^S are very close to the SM values. On the other hand, we show in Table II the other local minima for various CPC fits. We can see that the CPC.III.3 fit indeed has another local minimum, which has a χ^2 very close to the true minimum, at which C_u^S, C_v, C_d^S, and C_ℓ^S are extremely close to their SM values while $\Delta S^\gamma = -0.85$.

IV. IMPLICATIONS ON THE MSSM SPECTRUM

In this section, we shall try to find the implications of the current Higgs signal strength data on the masses of charginos, sleptons, sbottoms, and stops, as well as the A parameters—SUSY spectrum—through the virtual effects. Supersymmetric particles can enter into the picture of the observed Higgs boson via (i) exotic decays, e.g., into neutralinos; (ii) contributions to ΔS^γ by charginos, sleptons, and squarks; and (iii) contributions to ΔS^g by squarks. Note that virtual effects are also present in κ_d.

Being different from the fits considered in the previous section, we restrict $\tan\beta$ to be larger than $1/2$ so that the top-quark Yukawa coupling is supposed to be perturbative and the one-loop contributions of the SUSY particles to the $H\gamma\gamma$ and Hgg vertices remain reliable. Furthermore, as we shall see, the best-fit values of the couplings are close to the SM ones, and, accordingly, we take the lightest Higgs state (H_1) for the observed Higgs boson with $M_{H_1} \sim 125.5$ GeV.

A comprehensive survey over the full parameter space of the MSSM is a demanding task requiring a large amount of computing time. Since we are in pursuit of the implications of the current Higgs data on the SUSY spectrum, we consider the following three representative fits instead of carrying out the comprehensive study:

(i) MSSM-1: Only with chargino contributions.
(ii) MSSM-2: Only with scalar-tau contributions.
(iii) MSSM-3: With all chargino, scalar-tau, sbottom, and stop contributions.

In the MSSM-1 fit, we assume all the scalar fermions are too heavy to affect the Higgs signal strengths, and the heavy scalar fermions can easily generate the lightest Higgs

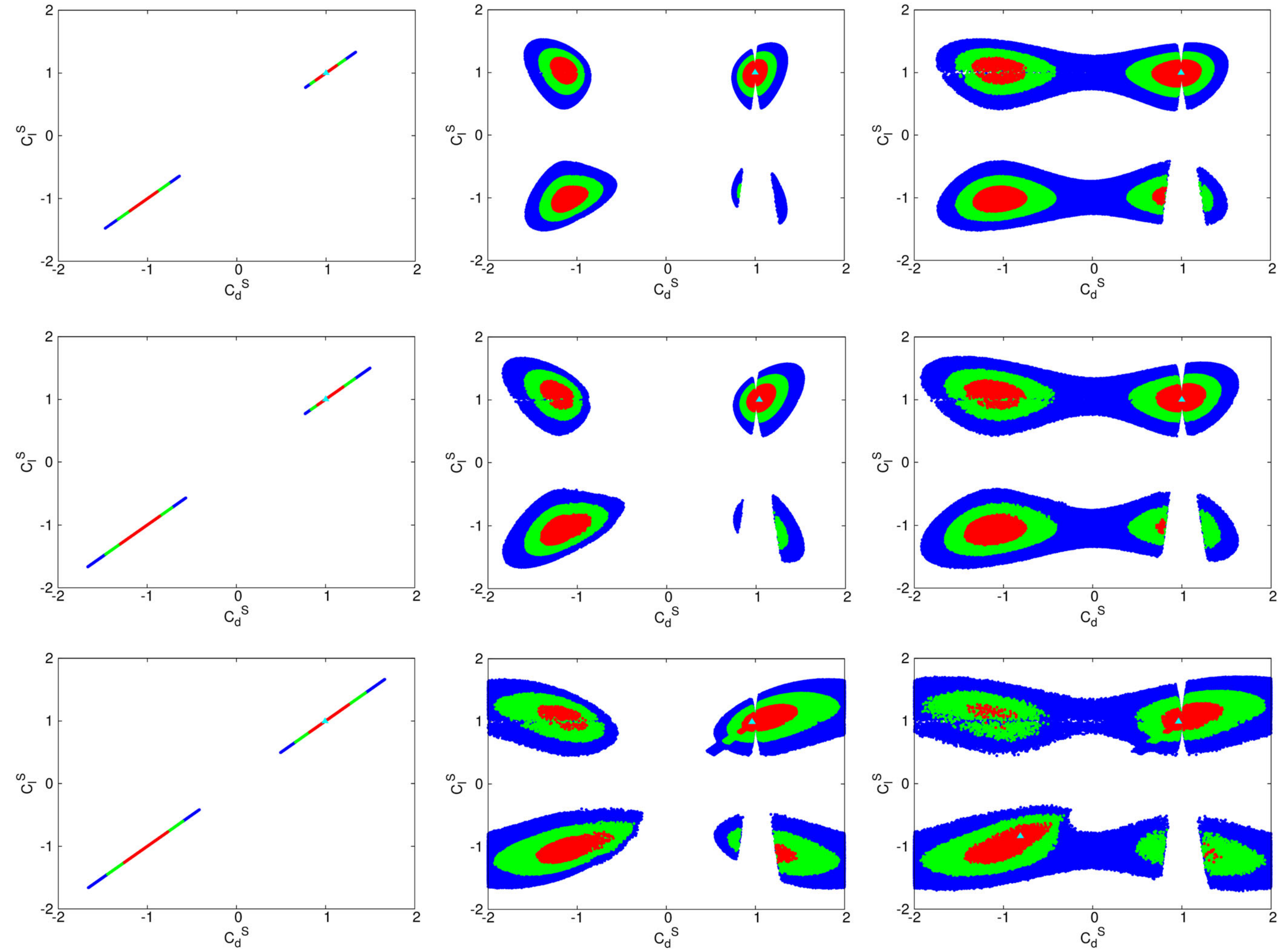

FIG. 5 (color online). The same as in Fig. 2 but on the (C_d^S, C_ℓ^S) plane.

boson weighing 125.5 GeV through the large renormalization group running effects, such as in split SUSY [60]. In this case, the lightest supersymmetric stable particle (LSP) is in general a mixed state of bino, wino, and Higgsinos.

In the MSSM-2 fit, except for the neutral LSP, we assume only the scalar taus are light enough to affect the Higgs signal strengths. Similar to the MSSM-1 case, the heavy stop and sbottoms can easily give $M_{H_1} \sim 125.5$ GeV. In this fit, we are assuming the charginos are heavy and, therefore, the LSP is binolike and its mass is fixed by the bino mass parameter M_1.

In the MSSM-3 fit, we consider all the chargino, scalar-tau, sbottom, and stop contributions. Being different from the previous two fits, the mass spectrum of the Higgs sector is closely correlated with the SUSY contributions to Higgs signal strengths. To calculate the lightest Higgs mass, we adopt the the approximated two-loop level analytical expression [61,62] which is precise enough for the purpose of the current study. For the heavier Higgses, we assume that they are decoupled or heavier than ~300 GeV. To be more specific, we are taking $M_A = 300$ GeV and require $|M_{H_1} - 125.5\ \mathrm{GeV}| \leq 6$ GeV, taking account of the ~3 GeV theoretical error of the lightest Higgs mass.

Note that the charginos and sleptons have negligible effects on the Higgs boson mass and thus we do not impose Higgs boson mass constraints in the MSSM-1 and MSSM-2 fits.

A. MSSM-1: Charginos only

We first investigate the effects of charginos. The lower mass limit of the chargino is 103.5 GeV, so that the only place that it can affect the Higgs boson is in the loop factor ΔS^γ. The MSSM parameters that affect the chargino mass and the interactions with the Higgs boson are M_2, μ, and $\tan\beta$, shown in Eqs. (13) and (14). We show in Fig. 9 the confidence regions when we vary C_u^S, $\tan\beta$, M_2, and μ with the additional constraint on the chargino mass:

$$M_{\tilde{\chi}^\pm} > 103.5\ \mathrm{GeV}.$$

The results are analogous to those of the CPC.III.3 case if we do not impose the chargino mass constraint and the

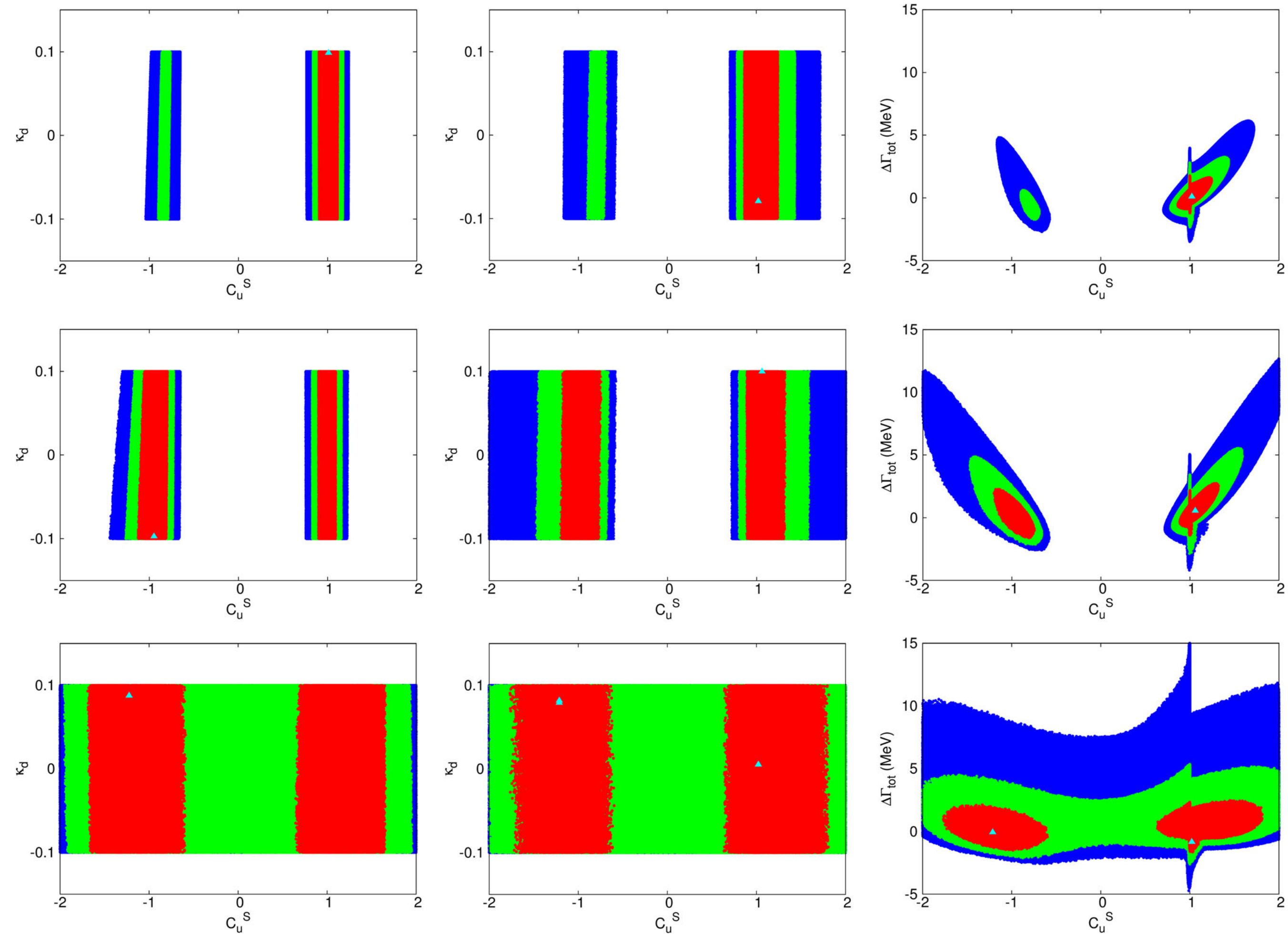

FIG. 6 (color online). The confidence-level regions on the (C_u^S, κ_d) (left and middle) and the (C_u^S, $\Delta\Gamma_{\rm tot}$) (right) planes. The left frames show the cases of CPC.II.3, CPC.III.4, and CPC.IV.5, and the middle and right frames are for the cases of CPC.II.4, CPC.III.5, and CPC.IV.6. The labeling of confidence regions is the same as in Fig. 2.

restriction of $\tan\beta > 1/2$. In the CPC.III.3 fit, ΔS^γ is free to vary both negatively and positively, while here the sign of the chargino contribution correlates with C_u^S in the parameter space of M_2 and μ. From the upper frames, we note that C_u^S is always positive under the requirement of $\tan\beta > 1/2$ and ΔS^γ tends to be positive taking its value in the range between -0.75 and 1.7 at 99.7% C.L. In the lower-left frame, we show the $M_{\tilde\chi_1^\pm}$ dependence of the C.L. regions of ΔS^γ. We observe that all the points fall into the 68.3% C.L. region of $-0.25 \lesssim \Delta S^\gamma \lesssim 0.43$ when $M_{\tilde\chi_1^\pm} \gtrsim 200$ GeV. We also observe that the μ parameter can be as low as 70 GeV when $M_2 < 0$ from the lower-right frame.

We show the best-fit point for the chargino contribution in Table III. The best-fit point gives $M_2 = 184$ GeV and $\mu = 179$ GeV, which give the lightest chargino mass $M_{\tilde\chi_1^\pm} = 103.7$ GeV, just above the current limit. The corresponding $\Delta S^\gamma \approx -0.68$. The p value is slightly worse than the CPC.III.3 case.

B. MSSM-2: Scalar taus

The staus contribute to ΔS^γ in a way similar to charginos. The SUSY soft parameters that affect the stau contributions are the left- and right-handed slepton masses M_{L_3} and M_{E_3}, the A parameter A_τ, and the μ parameter. We are taking $\mu > 1$ TeV to avoid possibly large chargino contributions to ΔS^γ. The 2×2 stau mass matrix is diagonalized to give two mass eigenstates $\tilde\tau_1$ and $\tilde\tau_2$, shown in (16) and (18). The current mass limit on the stau is $M_{\tilde\tau_1} > 81.9$ GeV [55].

We show in Fig. 10 the confidence regions when we vary C_u^S, $\tan\beta$, $M_{L_3} = M_{E_3}$, μ, and A_τ. Requiring $\tan\beta > 1/2$, $C_u^S > 0$ and most allowed regions are concentrated at $C_u^S \approx 1$ and $\Delta S^\gamma < 0$. Similar to the chargino case, C_u^S and ΔS^γ correlate with each other in the parameter space. The "T" shape of the C.L. regions of ΔS^γ (upper right) can be understood by observing that C_v is constrained to be very close to 1 unless $C_u^S \approx 1$ when $C_u^S > 0$; see the CPC.III (middle) frames of Fig. 3. We observe that all the points

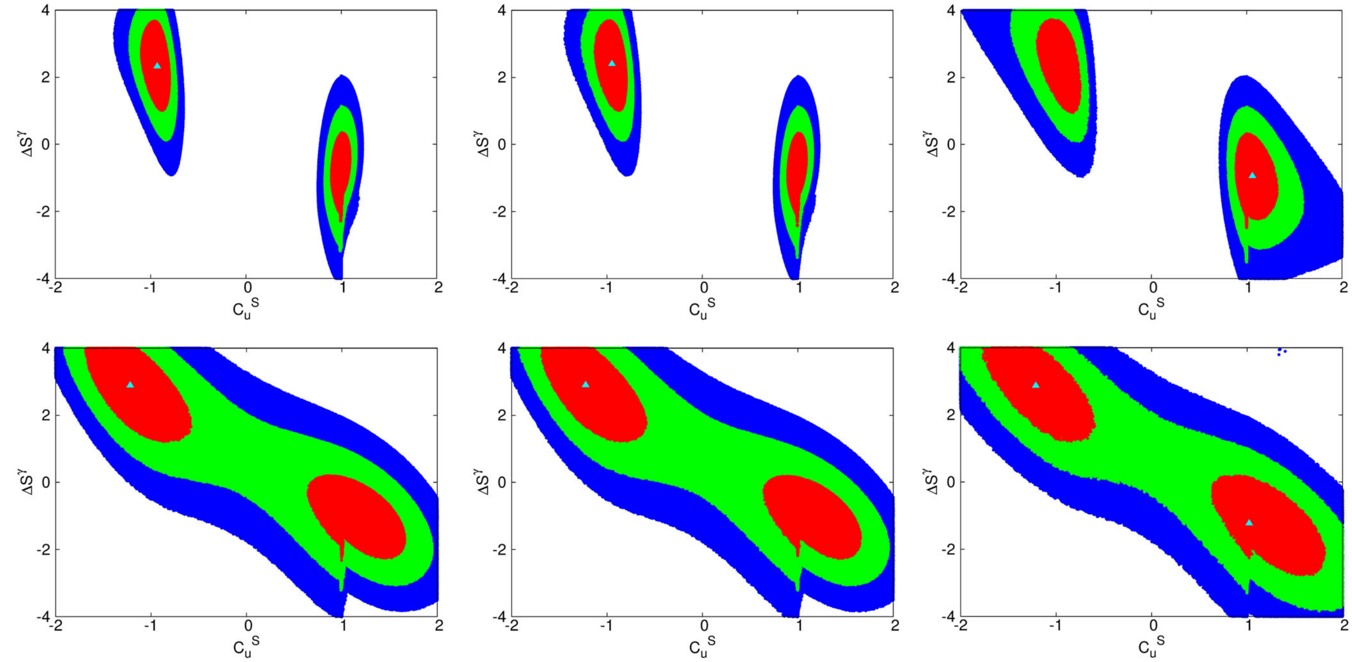

FIG. 7 (color online). The upper frames show the confidence-level regions on the $(C_u^S, \Delta S^\gamma)$ plane for the CPC.III.3 (left), CPC.III.4 (middle), and CPC.III.5 (right) fits. The lower frames are for the CPC.IV.4 (left), CPC.IV.5 (middle), and CPC.IV.6 (right) fits. The labeling of confidence regions is the same as in Fig. 2.

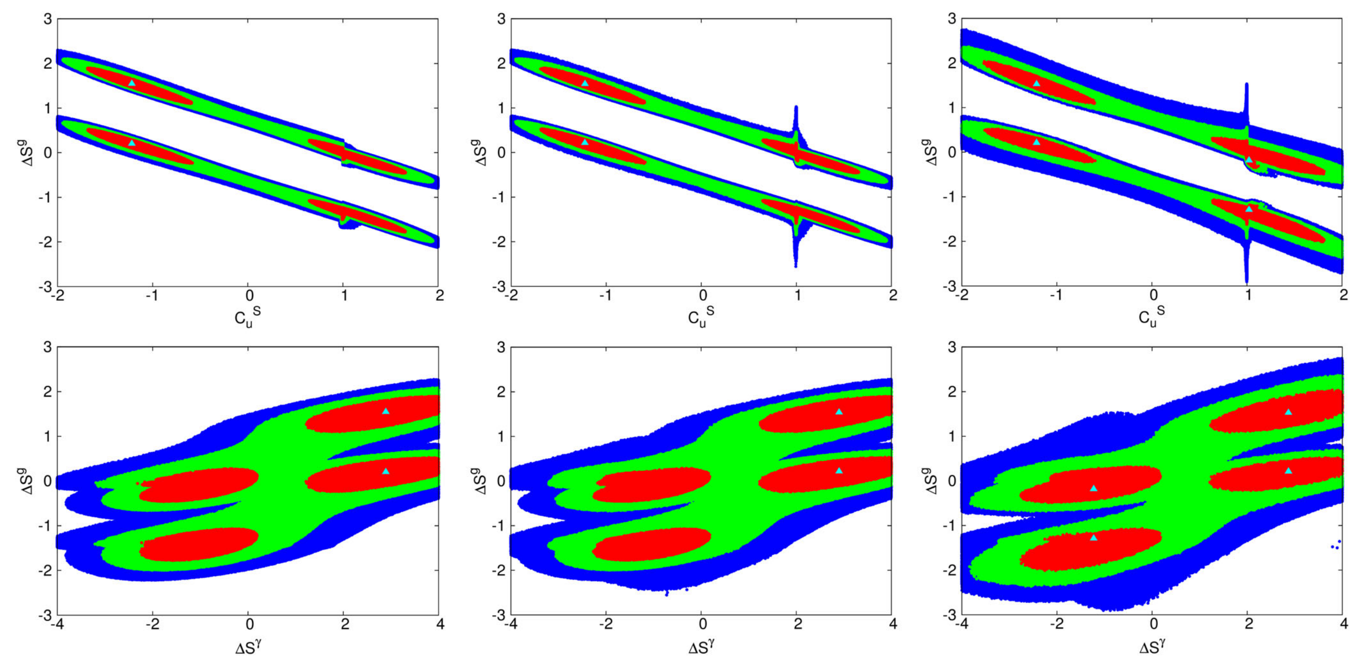

FIG. 8 (color online). The confidence-level regions on the $(C_u^S, \Delta S^g)$ (upper) and the $(\Delta S^\gamma, \Delta S^g)$ (lower) planes for the CPC.IV.4 (left), CPC.IV.5 (middle), and CPC.IV.6 (right) fits. The labeling of confidence regions is the same as in Fig. 2.

fall into the 68.3% C.L. region of $-1.8 \lesssim \Delta S^\gamma \lesssim 0$ when $M_{\tilde{\tau}_1} \gtrsim 180$ GeV.

The best-fit values are shown in Table IV. The χ^2 is just slightly worse than that of the CPC.III.3 case, and the p value is lowered because of more varying parameters. The values for C_u^S, C_v, C_ℓ^S, and C_d^S are very close to their SM values. The lightest stau has a mass of 132.3 GeV.

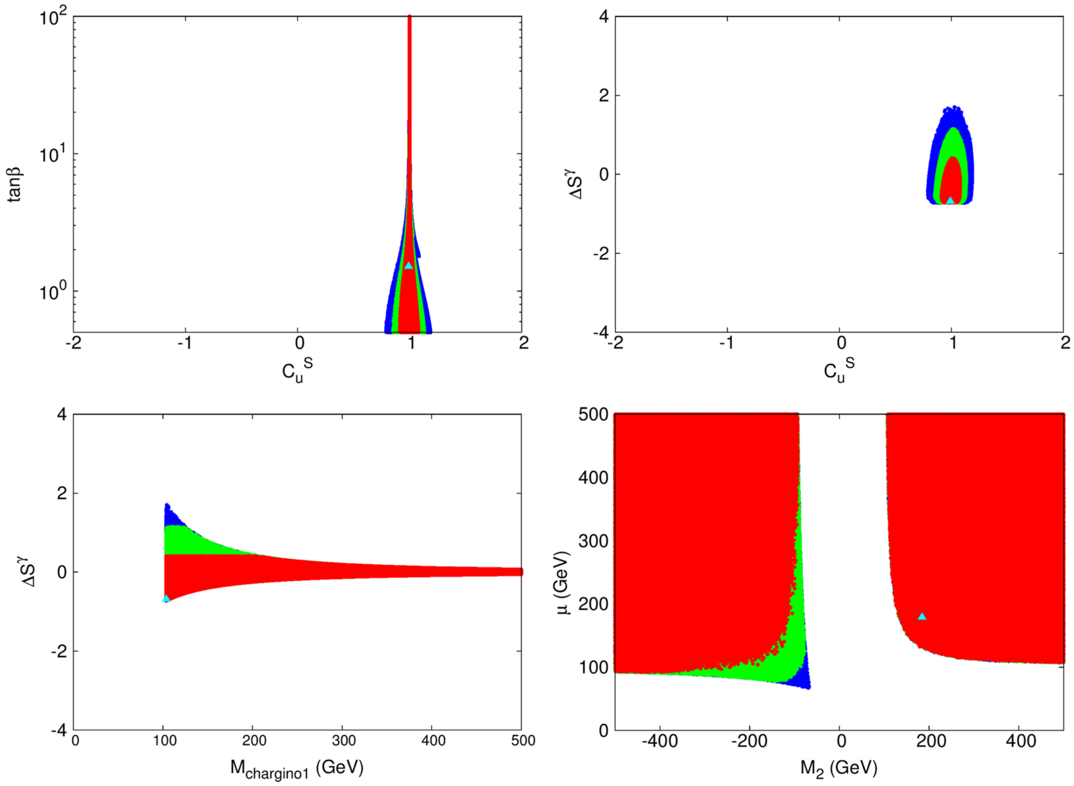

FIG. 9 (color online). MSSM-1 (charginos): The confidence-level regions of the fit by varying C_u^S, $\tan\beta$, M_2, and μ with $\tan\beta > 1/2$ and $M_{\tilde{\chi}_1^\pm} > 103.5$ GeV. The description of the confidence regions is the same as in Fig. 2.

C. MSSM-3: With all chargino, scalar tau, sbottom, and stop contributions

Here we include all contributions from charginos, scalar taus, sbottoms, and stops. The relevant SUSY soft parameters are $M_{Q_3}, M_{U_3}, M_{D_3}, M_{L_3}, M_{E_3}, A_t, A_b, A_\tau, M_3, M_2$, and M_A. In addition to C_u^S and $\tan\beta$, we are varying M_{Q_3}, M_{L_3}, A_t, and μ while taking $M_{Q_3} = M_{U_3} = M_{D_3}$, $M_{L_3} = M_{E_3}$, $A_t = A_b = A_\tau$, and $M_2 = \pm\mu$. We fix the other parameters as $M_3 = 1$ TeV and $M_A = 300$ GeV. Furthermore, we impose the following constraints on the masses:

$$M_{\tilde{\chi}_1^\pm} > 103.5 \text{ GeV}, \qquad M_{\tilde{\tau}_1} > 81.9 \text{ GeV},$$
$$M_{\tilde{t}_1} > 95.7 \text{ GeV}, \qquad M_{\tilde{b}_1} > 89 \text{ GeV},$$
$$|M_{H_1} - 125.5 \text{ GeV}| \le 6 \text{ GeV}.$$

Note that we adopt rather loose mass limits quoted in PDG [55] and impose the Higgs-boson mass constraint.

The best-fit values are shown in Table V. Note that the lighter stau mass (94.5 GeV) is near to its low mass limit, while all other SUSY particles are heavy, so that the major contribution to ΔS^γ is from the lighter stau as shown in the middle-right frame of Fig. 11. We observe that the stau contribution becomes comparable to that of the chargino around $M_{\tilde{\tau}_1} = 270$ GeV. For the larger values of $M_{\tilde{\tau}_1}$, ΔS^γ is saturated to have the values between ~ -0.6 and ~ 0.4 at 68% C.L. where it is dominated by the chargino loops.

The confidence regions in the relevant parameter space are shown in Fig. 11. From the upper-left frame of Fig. 11, we observe the requirement of $M_{H_1} \sim 125.5$ GeV

TABLE III. The best-fit values for chargino contributions to $\Delta S^\gamma(\tilde{\chi}_1^\pm, \tilde{\chi}_2^\pm)$. We imposed $M_{\tilde{\chi}_1^\pm} > 103.5$ GeV and $\tan\beta > 1/2$. The parameters C_u^S, $\tan\beta$, $M_2 \subset [-1\text{ TeV}, 1\text{ TeV}]$, and $\mu \subset [0, 1\text{ TeV}]$ are scanned.

				Best-fit values					
Fits	χ^2	χ^2/dof	p value	C_u^S	$\tan\beta$	κ_d	ΔS^γ	ΔS^g	$\Delta\Gamma_{\rm tot}$
Charginos	15.78	0.631	0.921	0.992	1.513	⋯	−0.683	⋯	⋯

Best-fit values						
C_v	C_d^S	C_ℓ^S	M_2 (GeV)	μ (GeV)	$M_{\tilde{\chi}_1^\pm}$ (GeV)	$M_{\tilde{\chi}_2^\pm}$ (GeV)
1.000	1.019	1.019	184	179	103.7	261.3

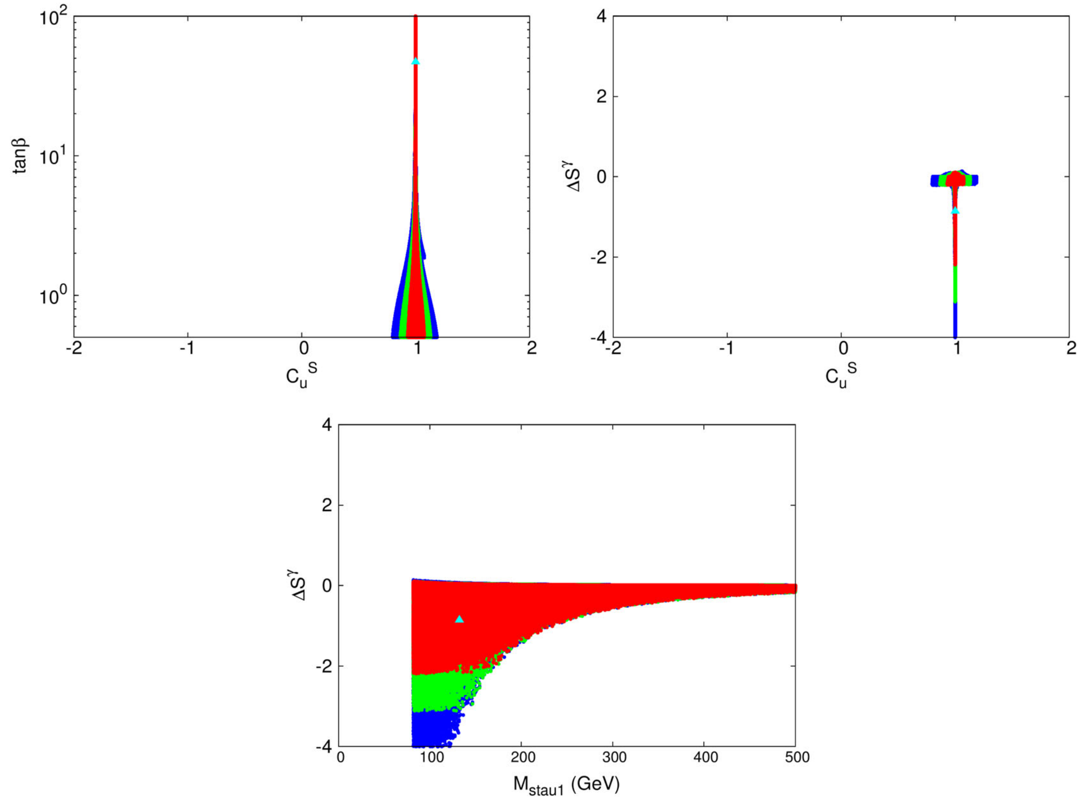

FIG. 10 (color online). MSSM-2 (staus): The confidence-level regions of the fit by varying C_u^S, $\tan\beta$, $M_{L_3} = M_{E_3}$, μ, and A_τ with the restrictions $\tan\beta > 1/2$, $\mu > 1$ TeV, and $M_{\tilde{\tau}_1} > 81.9$ GeV. The description of the confidence regions is the same as in Fig. 2.

completely removes the negative C_u^S region with $|C_u^S - 1| \lesssim 0.02$ and $\tan\beta \gtrsim 3$ at 95% C.L.

The majority of allowed parameter space is concentrated at around $C_u^S \approx 1$, $-2 \lesssim \Delta S^\gamma \lesssim 0$, and $\Delta S^g \approx 0$. Yet, there is a small island allowed at 99.7% C.L. around $\Delta S^\gamma \sim -3.5$ and $\Delta S^g \sim -1.5$. To identify the origin of the island, we note the following linear relationships between ΔS^γ and ΔS^g:

$$\Delta S^\gamma = 2N_C Q_b^2 \Delta S^g = \frac{2}{3}\Delta S^g \quad \text{for sbottom},$$

$$\Delta S^\gamma = 2N_C Q_t^2 \Delta S^g = \frac{8}{3}\Delta S^g \quad \text{for stop}.$$

In the chargino and stau cases, $\Delta S^g = 0$. These four correlations are represented by the straight lines in the upper-right frame of Fig. 11. It is clear that the island is due to the stop loops, and it disappears completely when we require either $M_{\tilde{t}_1} \gtrsim 150$ GeV or $M_{\tilde{b}_1} \gtrsim 450$ GeV, as shown in the lower frames.

To examine how large the squark contributions are or to suppress the relatively dominant stau and chargino contributions, we take $M_{\tilde{\chi}_1^\pm} > 300$ GeV and $M_{\tilde{\tau}_1} > 300$ GeV and show the results in Fig. 12. We observe that $|\Delta S^\gamma| \lesssim 0.6$ at 68.3% C.L. independently of the squark masses. This means that $|\Delta S^\gamma / S^\gamma_{\rm SM}| \lesssim 0.1$ with $S^\gamma_{\rm SM} \simeq -6.6$. Therefore, unless the $H\gamma\gamma$ coupling is determined with a precision better than 10%, this may imply that the Higgs data are not sensitive to the MSSM spectrum at 68.3% C.L. when

TABLE IV. The best-fit values for stau contributions to $\Delta S^\gamma(\tilde{\tau}_1, \tilde{\tau}_2)$. We set $M_{E_3} = M_{L_3}$ and imposed $\tan\beta > 1/2$, $\mu > 1$ TeV, and $M_{\tilde{\tau}_1} > 81.9$ GeV. The scanning parameters are C_u^S, $\tan\beta$, $M_{L_3} \subset [0, 1$ TeV$]$, $\mu \subset [1, 2$ TeV$]$, and $A_\tau \subset [-1$ TeV$, 1$ TeV$]$.

				Best-fit values					
Fits	χ^2	χ^2/dof	p value	C_u^S	$\tan\beta$	κ_d	ΔS^γ	ΔS^g	$\Delta\Gamma_{\rm tot}$
Scalar taus	15.68	0.653	0.899	1.000	47.14	⋯	−0.854	⋯	⋯

Best-fit values							
C_v	C_d^S	C_ℓ^S	M_{L_3} (GeV)	μ (GeV)	A_τ (GeV)	$M_{\tilde{\tau}_1}$ (GeV)	$M_{\tilde{\tau}_2}$ (GeV)
1.000	1.040	1.040	323	1075	−43.2	132.3	442.4

TABLE V. The chargino, scalar tau, sbottom, and stop contributions to $\Delta S^\gamma(\tilde\chi_1^\pm, \tilde\chi_2^\pm, \tilde\tau_1, \tilde\tau_2, \tilde b_1, \tilde b_2, \tilde t_1, \tilde t_2)$, $\Delta S^g(\tilde b_1, \tilde b_2, \tilde t_1, \tilde t_2)$, κ_d. We are taking $M_{L_3} = M_{E_3}$, $M_{Q_3} = M_{U_3} = M_{D_3}$, $A_t = A_b = A_\tau$, $M_3 = 1$ TeV, $M_A = 300$ GeV, $M_2 = \pm\mu$, and imposing mass limits $|M_{H_1} - 125.5\ \mathrm{GeV}| \le 6$ GeV, $M_{\tilde\chi_1^\pm} > 103.5$ GeV, $M_{\tilde\tau_1} > 81.9$ GeV, $M_{\tilde t_1} > 95.7$ GeV, and $M_{\tilde b_1} > 89$ GeV. Scanning parameters: C_u^S, $\tan\beta \subset [1, 100]$, $M_{L_3} \subset [0, 2\ \mathrm{TeV}]$, $M_{Q_3} \subset [0, 2\ \mathrm{TeV}]$, $\mu \subset [0, 2\ \mathrm{TeV}]$, $A_t \subset [-6\ \mathrm{TeV}, 6\ \mathrm{TeV}]$.

				Best-fit values					
Fits	χ^2	χ^2/dof	p value	C_u^S	$\tan\beta$	κ_d	ΔS^γ	ΔS^g	$\Delta\Gamma_{\rm tot}$
All SUSY	15.68	0.682	0.869	1.000	16.85	0.002	−0.846	0.001	–

Best-fit values														
C_v	C_d^S	C_ℓ^S	M_{L_3}	M_{Q_3}	M_2	A_t	$M_{\tilde\chi_1^\pm}$	$M_{\tilde\chi_2^\pm}$	$M_{\tilde\tau_1}$	$M_{\tilde\tau_2}$	$M_{\tilde t_1}$	$M_{\tilde t_2}$	$M_{\tilde b_1}$	$M_{\tilde b_2}$
1.000	1.040	1.041	220	1732	−1255	−2218	1203	1310	94.5	303	1640	1829	1717	1748

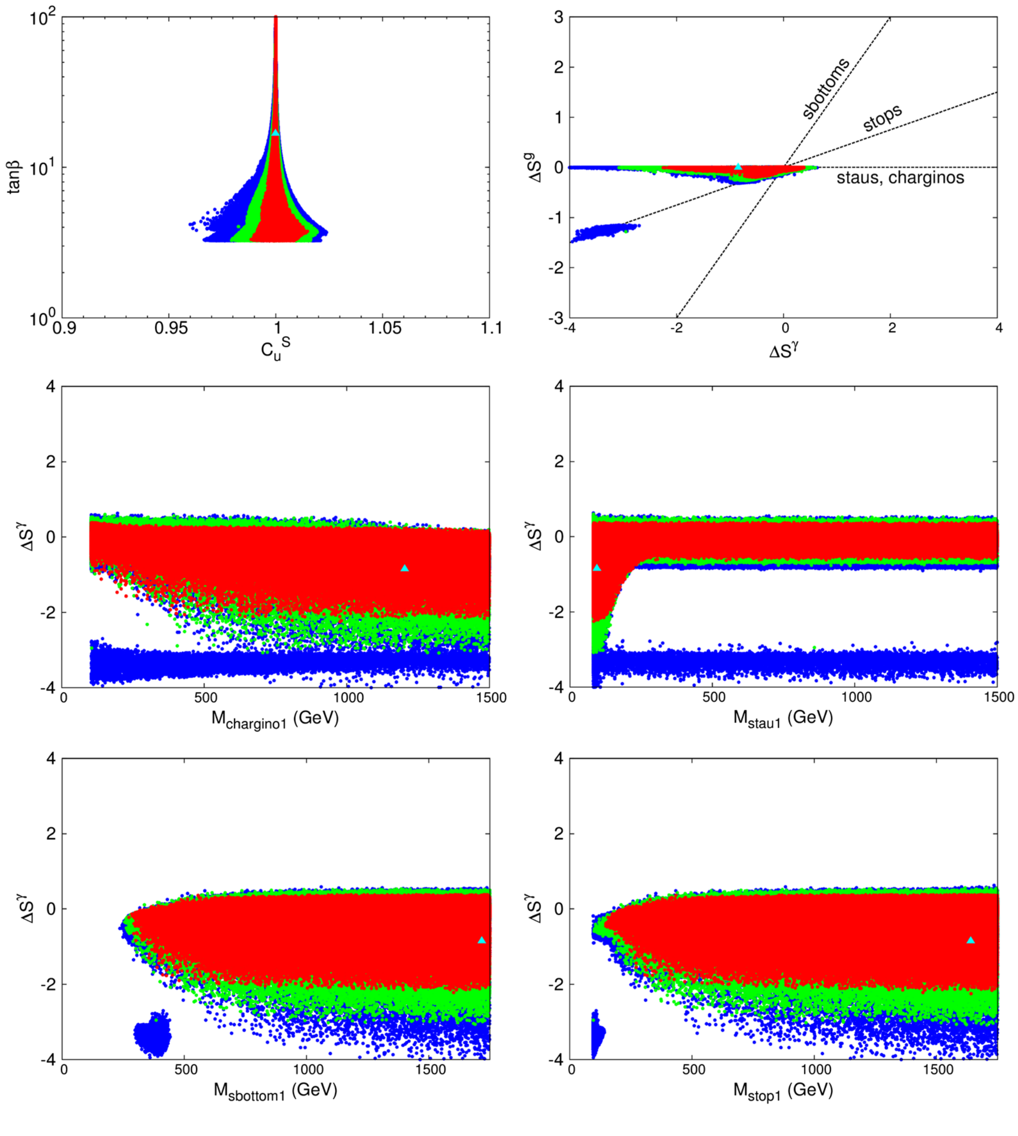

FIG. 11 (color online). MSSM-3 (all-SUSY particles): The confidence-level regions of the fit by varying C_u^S, $\tan\beta$, $M_{Q_3} = M_{U_3} = M_{D_3}$, $M_{L_3} = M_{E_3}$, $A_t = A_b = A_\tau$, μ with $M_3 = 1$ TeV, $M_A = 300$ GeV, $M_2 = \pm\mu$, and imposing mass limits $|M_{H_1} - 125.5\ \mathrm{GeV}| \le 6$ GeV, $M_{\tilde\chi_1^\pm} > 103.5$ GeV, $M_{\tilde\tau_1} > 81.9$ GeV, $M_{\tilde t_1} > 95.7$ GeV, and $M_{\tilde b_1} > 89$ GeV. The description of the confidence regions is the same as in Fig. 2.

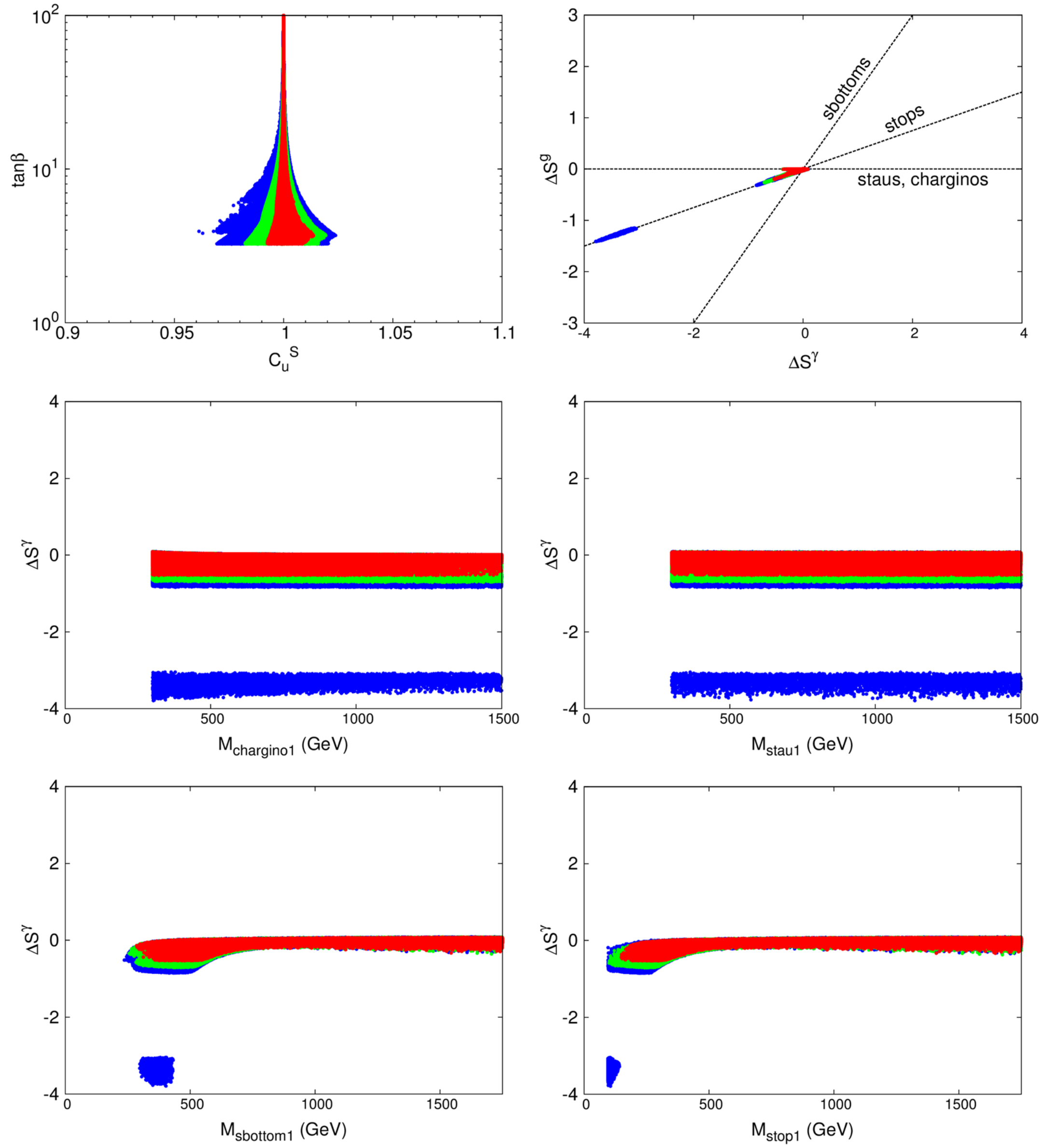

FIG. 12 (color online). MSSM-3 (all-SUSY particles): The same as Fig. 11 but requiring $M_{\tilde{\chi}_1^\pm} > 300$ GeV and $M_{\tilde{\tau}_1} > 300$ GeV.

$M_{\tilde{\chi}_1^\pm} > 300$ GeV and $M_{\tilde{\tau}_1} > 300$ GeV independently of the stop and sbottom masses. Incidentally, in the middle frames, we observe that the C.L. regions of ΔS^γ are almost independent of $M_{\tilde{\chi}_1^\pm,\tilde{\tau}_1}$ since they are dominated by the squark loops when $M_{\tilde{\chi}_1^\pm,\tilde{\tau}_1} > 300$ GeV.

Furthermore, we observe that the stau and chargino contributions decrease quickly as their masses increase, as shown in the previous MSSM-1 and MSSM-2 fits. Also, it is worth noting that $|\Delta S^\gamma| \lesssim 0.2$ when $M_{\tilde{\chi}_1^\pm,\tilde{\tau}_1} > 500$ GeV; see Figs. 9 and 10 when squarks are very heavy.

Finally, we also find that $|\Delta S^\gamma| \lesssim 0.2$ if we take the current 95% C.L. LHC limits on the stop and sbottom masses with $M_{\tilde{\chi}_1^0} = 0$ GeV [55]; $M_{\tilde{t}_1} > 650$ GeV and $M_{\tilde{b}_1} > 600$ GeV, assuming that charginos and staus are heavy enough and do not contribute to $|\Delta S^\gamma|$ more significantly than squarks.

Before concluding, we would like to briefly discuss the SUSY impact on future measurements of the Higgs properties through the Higgs decay into $Z\gamma$ and the Higgs cubic coupling. In the MSSM-1 case, thanks to light charginos, we have found that the branching ratio of the 125 GeV Higgs boson to $Z\gamma$ can be enhanced by about 15% compared to the SM prediction. On the other hand, in the MSSM-2 and MSSM-3 cases, the SUSY contribution to the branching ratio is less than 1%. Meanwhile, in the MSSM-3 case in which all the masses of relevant SUSY particles are specified and an unambiguous estimation of the Higgs cubic coupling is possible, the deviation of the Higgs cubic coupling from the SM value $M_{H_1}^2/2v$

($v \approx 246$ GeV) is negligible upon its variation according to the Higgs mass constraint taken in this work: $|M_{H_1} - 125.5\ \text{GeV}| < 6$ GeV.

V. SYNOPSIS AND CONCLUSIONS

We have analyzed the relevant parameter space in the MSSM with respect to the most updated data on the Higgs boson signal strength. The analysis is different from the model-independent one [4] mainly because ΔS^γ and ΔS^g are related by a simple relation, and up-type, down-type, and leptonic Yukawa couplings are also related to one another, such that they are no longer independent. We have shown in Figs. 1 to 8 the confidence-level regions in the parameter space for the cases of CPC.II to CPC.IV fits by varying a subset or all of the following parameters: C_u^S, $\tan\beta$ (or equivalently C_v), κ_d, ΔS^γ, ΔS^g, and $\Delta\Gamma_{\text{tot}}$. This set of parameters is inspired by the parameters of the general MSSM. Since the Higgs sector of the MSSM is the same as the 2HDM Type II, the down-type and the leptonic Yukawa couplings are determined once the up-type Yukawa couplings are fixed. It implies that C_u^S and $\tan\beta$ (or equivalently C_v) can determine all the tree-level Yukawa and gauge-Higgs couplings. The effects of the SUSY spectrum then enter into the parameters κ_d, ΔS^γ, and ΔS^g through loops of colored and charged particles.

There are improvements in all the CPC fits since our analysis of 2HDM [40] a year ago. The most significant changes in the Higgs-boson data from 2013 to 2014 were the diphoton signal strengths measured by both ATLAS and CMS [58,59], while all other channels were moderately improved. Overall, all fitted couplings are improved by about 10%, and the SM Higgs boson enjoys a large p value close to 1 [4].

The SUSY particles enter the analysis mainly through the loop effects of the colored and charged particles into the parameters such as ΔS^γ, ΔS^g, and κ_d, while light neutralinos with mass less than $M_{H_1}/2$ can enter into $\Delta\Gamma_{\text{tot}}$. We have analyzed the effects of the SUSY spectrum with the direct search limits quoted in PDG [55]. We offer the following comments concerning the MSSM spectrum:

(1) The effect of κ_d on the C.L. regions is insignificant, which can be seen easily when we go across from the first column to the second column in Figs. 2 to 4. On the other hand, the effect of $\Delta\Gamma_{\text{tot}}$ is relatively large, which can be seen by going across from the second column to the last column in Figs. 2 to 4.

(2) Since the mass of the lightest Higgs boson is sensitive to the stop mass, we especially impose the current Higgs-boson mass limit $M_{H_1} \sim 125.5 \pm 6$ GeV (taking on a roughly 3-σ level) on the parameter space in the MSSM-3 fits with all-SUSY particles. There are always some underlying assumptions on deriving the mass limits of stops and sbottoms (also true for other SUSY particles). We have imposed mild but robust mass limits.

(3) The MSSM-1 (chargino) and MSSM-2 (stau) fits are special cases of CPC.III.3 in which $\tan\beta$ (or equivalently C_v), C_u^S, and ΔS^γ are varied. Nevertheless, the ΔS^γ is restricted by the SUSY parameters μ, $\tan\beta$, and M_2 or M_{L_3,E_3} in such a way that ΔS^γ is not entirely free to vary. The resulting fits are not as good as the CPC.III.3 case.

(4) In the MSSM-3 case in which we consider the chargino, stau, stop, and sbottom contributions, the preferred C_u^S is very close to 1. The major contribution comes from the lightest stau, which stands very close to the low mass limit of 81.9 GeV.

(5) The direct search limits on charginos and staus prevent the ΔS^γ from becoming too large, while those on stops and sbottoms prevent both ΔS^γ and ΔS^g from becoming too large.

(6) We find that $|\Delta S^\gamma / S^\gamma_{\text{SM}}| \lesssim 0.1$ when $M_{\tilde{\chi}_1^\pm} > 300$ GeV and $M_{\tilde{\tau}_1} > 300$ GeV, irrespective of the squarks masses. Note that $S^\gamma_{\text{SM}} \simeq -6.6$.

(7) Further we observe that $|\Delta S^\gamma / S^\gamma_{\text{SM}}| \lesssim 0.03$ when $M_{\tilde{\chi}_1^\pm, \tilde{\tau}_1} > 500$ GeV and $M_{\tilde{t}_1, \tilde{b}_1} \gtrsim 600$ GeV.

ACKNOWLEDGMENTS

This work was supported the National Science Council of Taiwan under Grant No. NSC 102-2112-M-007-015-MY3. J. S. L. was supported by the National Research Foundation of Korea Grant No. 2013R1A2A2A01015406. This study was also financially supported by Chonnam National University, 2012.

[1] G. Aad *et al.* (ATLAS Collaboration), Phys. Lett. B **716**, 1 (2012).
[2] S. Chatrchyan *et al.* (CMS Collaboration), Phys. Lett. B **716**, 30 (2012).
[3] K. Cheung, J. S. Lee, and P.-Y. Tseng, J. High Energy Phys. 05 (2013) 134.
[4] K. Cheung, J. S. Lee, and P. Y. Tseng, Phys. Rev. D **90**, 095009 (2014).
[5] P. W. Higgs, Phys. Rev. Lett. **13**, 508 (1964); F. Englert and R. Brout, Phys. Rev. Lett. **13**, 321 (1964); G. S. Guralnik, C. R. Hagen, and T. W. B. Kibble, Phys. Rev. Lett. **13**, 585 (1964).

[6] D. Carmi, A. Falkowski, E. Kuflik, and T. Volansky, J. High Energy Phys. 07 (2012) 136.
[7] A. Azatov, R. Contino, and J. Galloway, J. High Energy Phys. 04 (2012) 127.
[8] J. R. Espinosa, C. Grojean, M. Muhlleitner, and M. Trott, J. High Energy Phys. 05 (2012) 097.
[9] M. Klute, R. Lafaye, T. Plehn, M. Rauch, and D. Zerwas, Phys. Rev. Lett. **109**, 101801 (2012).
[10] D. Carmi, A. Falkowski, E. Kuflik, and T. Volansky, Nuovo Cimento C **035**, 315 (2012).
[11] I. Low, J. Lykken, and G. Shaughnessy, Phys. Rev. D **86**, 093012 (2012).
[12] P. P. Giardino, K. Kannike, M. Raidal, and A. Strumia, Phys. Lett. B **718**, 469 (2012).
[13] J. Ellis and T. You, J. High Energy Phys. 09 (2012) 123.
[14] J. R. Espinosa, C. Grojean, M. Muhlleitner, and M. Trott, J. High Energy Phys. 12 (2012) 045.
[15] D. Carmi, A. Falkowski, E. Kuflik, T. Volansky, and J. Zupan, J. High Energy Phys. 10 (2012) 196.
[16] S. Banerjee, S. Mukhopadhyay, and B. Mukhopadhyaya, J. High Energy Phys. 10 (2012) 062.
[17] F. Bonnet, T. Ota, M. Rauch, and W. Winter, Phys. Rev. D **86**, 093014 (2012).
[18] T. Plehn and M. Rauch, Europhys. Lett. **100**, 11002 (2012).
[19] A. Djouadi, Eur. Phys. J. C **73**, 2489 (2013).
[20] B. A. Dobrescu and J. D. Lykken, J. High Energy Phys. 02 (2013) 073.
[21] G. Cacciapaglia, A. Deandrea, G. D. La Rochelle, and J.-B. Flament, J. High Energy Phys. 03 (2013) 029.
[22] G. Belanger, B. Dumont, U. Ellwanger, J. F. Gunion, and S. Kraml, J. High Energy Phys. 02 (2013) 053.
[23] G. Moreau, Phys. Rev. D **87**, 015027 (2013).
[24] T. Corbett, O. J. P. Eboli, J. Gonzalez-Fraile, and M. C. Gonzalez-Garcia, Phys. Rev. D **86**, 075013 (2012).
[25] T. Corbett, O. J. P. Eboli, J. Gonzalez-Fraile, and M. C. Gonzalez-Garcia, Phys. Rev. D **87**, 015022 (2013).
[26] E. Masso and V. Sanz, Phys. Rev. D **87**, 033001 (2013).
[27] E. Boos, V. Bunichev, M. Dubinin, and Y. Kurihara, Phys. Rev. D **89**, 035001 (2014).
[28] J. Ellis, V. Sanz, and T. You, J. High Energy Phys. 07 (2014) 036.
[29] R. Edezhath, arXiv:1501.00992.
[30] H. S. Cheon and S. K. Kang, J. High Energy Phys. 09 (2013) 085.
[31] N. Craig and S. Thomas, J. High Energy Phys. 11 (2012) 083.
[32] D. S. M. Alves, P. J. Fox, and N. J. Weiner, arXiv: 1207.5499.
[33] W. Altmannshofer, S. Gori, and G. D. Kribs, Phys. Rev. D **86**, 115009 (2012).
[34] S. Chang, S. K. Kang, J.-P. Lee, K. Y. Lee, S. C. Park, and J. Song, J. High Energy Phys. 05 (2013) 075.
[35] Y. Bai, V. Barger, L. L. Everett, and G. Shaughnessy, Phys. Rev. D **87**, 115013 (2013).
[36] A. Drozd, B. Grzadkowski, J. F. Gunion, and Y. Jiang, J. High Energy Phys. 05 (2013) 072.
[37] A. Celis, V. Ilisie, and A. Pich, J. High Energy Phys. 07 (2013) 053.
[38] V. Barger, L. L. Everett, H. E. Logan, and G. Shaughnessy, Phys. Rev. D **88**, 115003 (2013).
[39] S. Chang, S. K. Kang, J.-P. Lee, K. Y. Lee, S. C. Park, and J. Song, J. High Energy Phys. 09 (2014) 101.
[40] K. Cheung, J. S. Lee, and P. Y. Tseng, J. High Energy Phys. 01 (2014) 085.
[41] A. Celis, V. Ilisie, and A. Pich, J. High Energy Phys. 12 (2013) 095.
[42] L. Wang and X.-F. Han, J. High Energy Phys. 11 (2014) 085.
[43] B. Dumont, J. F. Gunion, Y. Jiang, and S. Kraml, Phys. Rev. D **90**, 035021 (2014).
[44] J. R. Espinosa, C. Grojean, V. Sanz, and M. Trott, J. High Energy Phys. 12 (2012) 077.
[45] A. Azatov, S. Chang, N. Craig, and J. Galloway, Phys. Rev. D **86**, 075033 (2012).
[46] P. Bechtle, S. Heinemeyer, O. Stal, T. Stefaniak, G. Weiglein, and L. Zeune, Eur. Phys. J. C **73**, 2354 (2013).
[47] J. Cao, Z. Heng, J. M. Yang, and J. Zhu, J. High Energy Phys. 10 (2012) 079.
[48] H. Baer, V. Barger, P. Huang, D. Mickelson, A. Mustafayev, and X. Tata, Phys. Rev. D **87**, 035017 (2013).
[49] A. Fowlie, M. Kazana, K. Kowalska, S. Munir, L. Roszkowski, E. M. Sessolo, S. Trojanowski, and Y.-L. Sming Tsai, Phys. Rev. D **86**, 075010 (2012).
[50] K. Hagiwara, J. S. Lee, and J. Nakamura, J. High Energy Phys. 10 (2012) 002.
[51] A. Arbey, M. Battaglia, A. Djouadi, and F. Mahmoudi, Phys. Lett. B **720**, 153 (2013).
[52] S. Scopel, N. Fornengo, and A. Bottino, Phys. Rev. D **88**, 023506 (2013).
[53] B. Dumont, J. F. Gunion, and S. Kraml, Phys. Rev. D **89**, 055018 (2014).
[54] K. Cheung, J. S. Lee, E. Senaha, and P. Y. Tseng, J. High Energy Phys. 06 (2014) 149.
[55] J. Beringer *et al.* (Particle Data Group), Phys. Rev. D **86**, 010001 (2012).
[56] J. S. Lee, A. Pilaftsis, M. S. Carena, S. Y. Choi, M. Drees, J. R. Ellis, and C. E. M. Wagner, Comput. Phys. Commun. **156**, 283 (2004); J. S. Lee, M. Carena, J. Ellis, A. Pilaftsis, and C. E. M. Wagner, Comput. Phys. Commun. **180**, 312 (2009); J. S. Lee, M. Carena, J. Ellis, A. Pilaftsis, and C. E. M. Wagner, Comput. Phys. Commun. **184**, 1220 (2013).
[57] F. Borzumati, J. S. Lee, and W. Y. Song, Phys. Lett. B **595**, 347 (2004).
[58] G. Aad *et al.* (ATLAS Collaboration), Phys. Rev. D **90**, 052004 (2014).
[59] V. Khachatryan *et al.* (CMS Collaboration), Eur. Phys. J. C **74**, 3076 (2014).
[60] G. F. Giudice and A. Strumia, Nucl. Phys. **B858**, 63 (2012).
[61] S. Heinemeyer, W. Hollik, and G. Weiglein, Phys. Lett. B **455**, 179 (1999).
[62] J. R. Espinosa and R. J. Zhang, Nucl. Phys. **B586**, 3 (2000).